Handling Performance Analysis of Run-Flat and Standard Tires Using Pacejka Tire Model

Anurag Mahajan

Thesis submitted to the faculty of the Virginia Polytechnic Institute and State University in partial fulfilment of the requirements for the degree of

Master of Science
In
Mechanical Engineering

Saied Taheri, Chair
Robert L. West
Jeffrey Thomas Warfford

June 9, 2025
Blacksburg, VA

Handling Performance Analysis of Run-Flat and Standard Tires Using Pacejka Tire Model

Anurag Mahajan

ABSTRACT

This thesis investigates the handling performance of standard pneumatic tires and self-supporting run-flat tires under deflation scenarios using a combined finite element and vehicle dynamics simulation approach. Finite element models of both tire types were developed in Abaqus to extract lateral force characteristics across slip angles (-4° to +4°) and inflation pressures (250 kPa, 130 kPa, and 0 kPa). The extracted data were fitted using the Pacejka Magic Formula, yielding peak lateral forces of up to 4162 N for inflated run-flat tires and 4769 N in the deflated state, compared to 3577 N and 4919 N for standard tires, respectively. These models were integrated into a double-track vehicle dynamics model with quasi-static lateral load transfer and a velocity-scaled path-following controller. Constant-radius turning maneuvers at 22 m/s were simulated with front-left tire deflation introduced at 13 seconds. Results showed that standard tires experienced over 10 meters of lateral deviation post-deflation, with saturated steering input, while run-flat tires limited deviation to under 0.5 meters and maintained control without reaching steering saturation. The study highlights the superior safety potential of run-flat tires under pressure-loss conditions and demonstrates the effectiveness of integrated finite element and empirical modelling in predicting vehicle handling performance during tire failure.

Handling Performance Analysis of Run-Flat and Standard Tires Using Pacejka Tire Model

Anurag Mahajan

GENERAL AUDIENCE ABSTRACT

Tires play a critical role in keeping vehicles safe and stable on the road, especially during emergencies like a sudden loss of air pressure. This study compares standard tires and special "run-flat" tires that are designed to keep working even after losing air. Using advanced computer models, we first simulated how these tires behave under normal and deflated conditions. We then tested how a car with these tires handles during high-speed turns and quick lane changes. The results showed that when a standard tire loses air, the car can veer dangerously off its path, with the steering system unable to correct the problem. In contrast, the run-flat tires helped the car stay much closer to its intended path, even after losing pressure, thanks to their stronger sidewalls that continue to support the vehicle. This research highlights how run-flat tires can make driving safer in the event of a tire failure and shows how computer simulations can help engineers design better tires and vehicles for everyday use.

Contents

List of Figures

1. Introduction

1.1 Motivation

Modern vehicle dynamics demand a high level of performance, safety, and comfort, especially under varying driving conditions. Tires play a critical role in transmitting forces between the road and the vehicle, and their behavior significantly influences both handling and ride quality. With increasing emphasis on run-flat tires due to their safety advantages—particularly the ability to operate temporarily after deflation, understanding their dynamic performance has become crucial. The self-supporting tires which enable run-flat functionality also to introduce a complex behavior in tire deformation and force generation directly affecting the overall vehicle dynamics. Lateral force generation and ride quality are not discussed widely in available literature as part of the performance of a run-flat tire. These handling parameters are important part of the overall performance and are explored in this work.

1.2 Thesis objectives

1. To simulate standard and self-supporting runflat tire models in deflated condition and extract tire forces generated in dynamic conditions.

2. Develop Pacejka tire model for the run-flat tire by fitting the Pacejka coefficients using the extracted force data

3. Develop a vehicle model to study the handling performance of standard and runflat tires in deflated conditions.

The present work adopts a sidewall-reinforced run-flat tire design based on the prior development by Abhishek (2024), specifically utilizing the 15 mm lower version, which incorporates an additional layer of stiff rubber compound starting at the lower edge of the

upper belt. This configuration was selected due to its favourable trade-off between stiffness and additional mass. The design was originally developed for a 14-inch tire and was scaled up in this study for the 18-inch application. This work uses the original 14-inch version for the handling study.

1.3 Thesis structure

Chapter 2 – Literature Review

Chapter 3 – Finite Element Modelling of Tires

Chapter 4 – Tire Modelling

Chapter 5 – Vehicle Models and Stability Controller

Chapter 6 – Results of Standard Tire vs. Run-Flat Tire in deflated conditions.

Chapter 7 – Conclusion and Future Work.

Chapter 8 – References

Chapter 9 - Appendix

2. Literature Review

2.1 What is the history of a tire?

The development of pneumatic tires dates to the 19th century, with early efforts focused on improving the comfort and performance of bicycles. The concept of an air-filled tire was first patented by Robert William Thomson in 1845, but it did not gain commercial traction until John Boyd Dunlop reintroduced and patented the first practical pneumatic tires in 1888 for bicycles, sparking widespread interest and adoption (1).

The transformation from rudimentary air-filled casings to advanced tire systems was marked by several technological milestones. Initially, reinforcement materials such as Irish flax and cotton were used, but over time these were replaced by man-made fibres including viscose rayon, nylon, and polyester, followed by steel cords for superior strength and durability.

The 1920s saw the introduction of balloon tires, which offered an ellipse shape instead of a regular circular tire, larger cross-sections, and lower pressures for improved ride comfort (2). In the 1950s, the tubeless tire was developed, with improvements in rim design, eliminating the need for an inner tube and reducing the risk of rapid deflation (3).The belted bias tire, introduced in the 1960s, further enhanced tread stability by incorporating belts over the bias plies.

A major turning point came with the commercialization of the radial tire. Although radial constructions were patented earlier, it was not until 1946 that Michelin introduced the Michelin X, the first successful radial tire for passenger vehicles. This design gained popularity in Europe and eventually gained popularity in the United States by the 1970s, owing to its superior performance in terms of wear, fuel efficiency, and high-speed stability (4).

2.2 Types of tires?

Tire construction methods have evolved over time to meet the increasing demands of durability, comfort, and performance across different vehicle categories. The most common types of pneumatic tires include bias (diagonal) tires, belted bias tires, and radial tires, each distinguished by the orientation of their reinforcement plies and internal structure.

Bias tires, also referred to as diagonal tires, are constructed with a sidewall that runs diagonally from bead to bead at alternating angles, typically less than 90 degrees to each other and to the tread centreline. This crisscross pattern creates a highly interconnected carcass structure, in which the tread and sidewall work in unison. Although bias tires are relatively simple in design and easy to manufacture which makes them cost-effective and still prevalent in heavy duty applications like trailers, farm equipment, and off-road conditions, they tend to suffer from higher rolling resistance and heat generation. This is due to inter-ply shear that occurs during deformation, which can also accelerate tread wear and reduce high-speed performance.

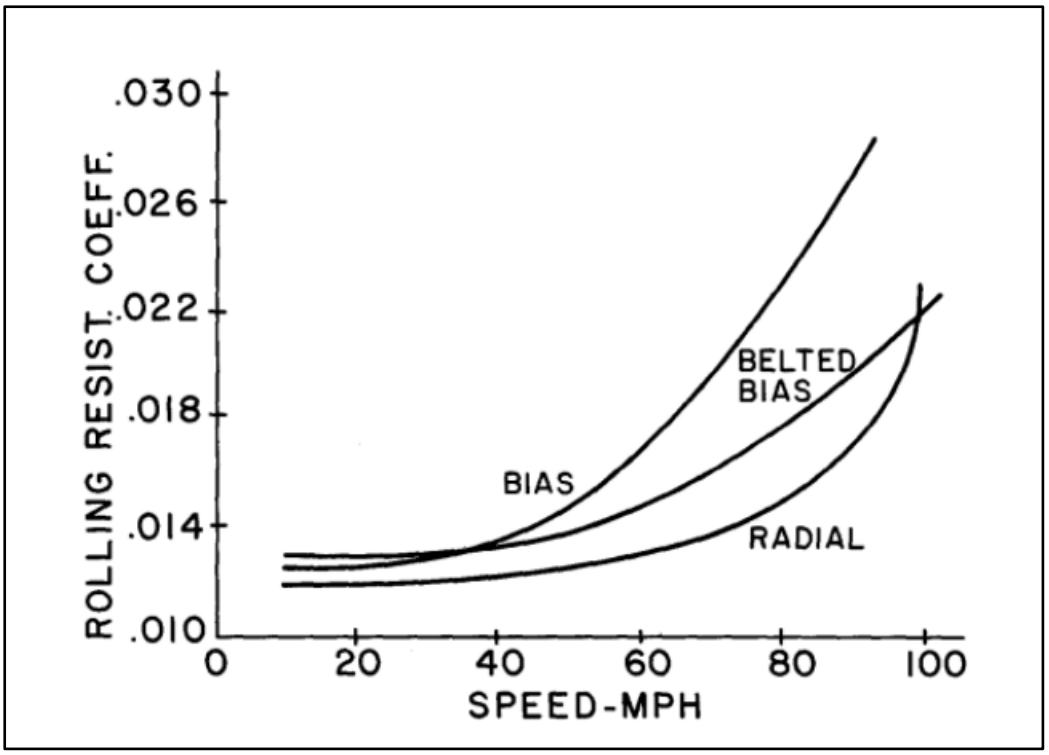

Figure 1: Rolling resistance coefficient as a function of speed for radial, belted bias, and bias tires. (5)

To address some of these limitations, belted bias tires incorporate one or more belt layer, also known as breaker plies, between the body plies and the tread. These belts are typically laid at low angles relative to the tread centreline and serve to reinforce the tread region by limiting circumferential expansion. The added belts contribute to improved tread stability owing to lower cord angle in the crown region, (6) better wear characteristics, and enhanced handling compared to conventional bias tires. However, since the fundamental bias construction remains unchanged, issues such as internal shear and heat buildup under dynamic loading persist, and the added complexity slightly increases production cost.

Radial tires, now the standard for most passenger and commercial vehicles, represent a significant advancement in tire design. In this configuration, the body plies are oriented radially, perpendicular to the tread centreline, extending straight across from bead to bead. Above these plies, two or more steel belts are positioned at opposing angles to provide rigidity and stability to the tread. The independent control over the stiffness of the crown and

the sidewall allows radial tires to deflect more easily in the sidewall while maintaining a stiff tread region, resulting in lower rolling resistance, improved fuel efficiency, better heat dissipation, and superior high-speed durability. Furthermore, the increased tread stiffness enhances handling, wear resistance, helps in a good response to steering with minimum sacrifice to ride comfort (7) Despite these advantages, the radial construction is more complex and requires advanced materials and manufacturing processes, which contribute to higher production costs.

2.3 What is a modern-day pneumatic tire?

A modern pneumatic tire is a highly engineered structural composite that acts as the interface between a vehicle and the road surface. It is a flexible, pressurized container composed of a complex blend of elastomers, textile or steel reinforcements, and chemical additives, designed to perform reliably under diverse loading and environmental conditions. The air pressure inside the tire is the primary load-bearing element, responsible for carrying approximately 90–95% of the vehicle load, while the remaining 5–10% is supported by the tire's structural stiffness (3)

The internal architecture of a radial tire comprises several key components, including the inner liner, carcass plies, bead bundles, belt plies, sidewalls, and the tread (8). Reinforcing cords made of polyester, nylon, or steel are embedded in rubber and aligned in specific orientations to resist tensile stresses. These carcass plies support internal pressure and contribute to the tire's structural form. Vulcanization, a chemical process involving sulphur or other curatives, transforms raw rubber into a durable, elastic material by creating cross-links between polymer chains, making the compound suitable for load-bearing applications.

Modern pneumatic tires are designed to meet a wide range of functional requirements essential for vehicle dynamics. These include load support, shock absorption, traction and

braking force transmission, lateral force generation during cornering, and dimensional stability (3). Additionally, tires are expected to provide low rolling resistance, resist environmental degradation, suppress noise and vibration, and maintain durability over their service life. All these functions are concentrated on the comparatively tiny contact patch, where combinations of normal and tangential forces are transferred between the tire and the road surface.

In high-performance and passenger vehicles, the standard tire configuration is the radial tubeless tire, typically featuring polyester carcass plies and steel belts. Recent developments include low aspect ratio tires, which have a wider section width relative to their height, offering improved cornering stiffness and handling response. Modern sidewalls are also imprinted with standardized markings that indicate critical parameters such as tire size, construction type, load index, speed rating, and wheel compatibility.

2.4 Construction of pneumatic tire

Pneumatic tires are a basic structural component for any vehicle serving as an interface between the vehicle and the road. They transmit forces related to acceleration, braking and cornering, while supporting vehicle's load and absorbing road irregularities. Radial tires are the highest used pneumatic tires for civilian vehicles due to superior performance characteristics in terms of handling, ride comfort and wear and tear. A radial tire has a complex, layered composite structure which consists of elastomeric and reinforcing materials which have individual structural and functional roles.

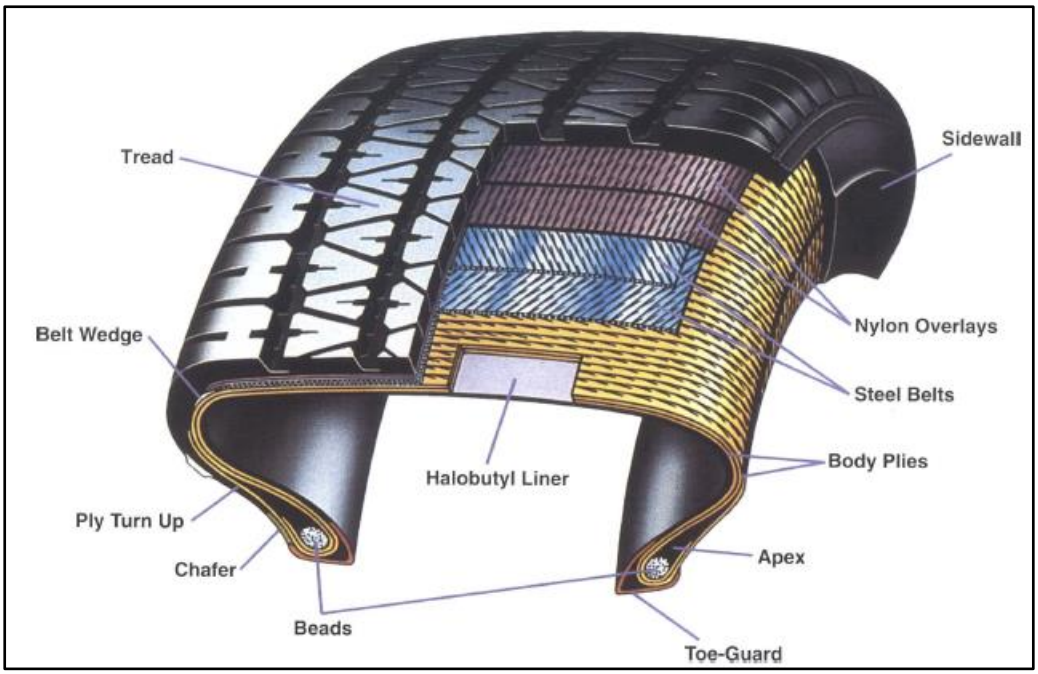

Figure 2: Cross section of passenger car tire (3).

The bead is the foundation of the tire, consisting of high-strength steel wire bundles that anchor the tire to wheel rim. The bead is encased by the bead filler or apex which is made from a stiff rubber compound, that influences ride and handling by modifying the stiffness gradient from the bead to the sidewall.

The body ply is made from polyester or nylon cords embedded in rubber which extends radially between two beads and acts as the main load bearing components. This provides the necessary structural integrity to the tire to contain internal pressure and to maintain tire shape under load. The body ply is protected along the sides by sidewall which protects the tire against abrasion, impacts, and environmental factors. The rubber compound in the sidewall is engineered for high fatigue resistance due to frequent flexing.

Above the body plies, the belt layers, usually consisting of two cross-laid steel belts, offer reinforcement beneath the tread. These belts stiffen the tread region, improve handling, and wear resistance, and contribute to overall tire stability by controlling tread deformation.

The tread is the only part of the tire in direct contact with the road. It is made of specially formulated rubber compound which provides optimal traction, wear resistance, fuel efficiency, and noise performance. The tread pattern is moulded during the curing process to channel water and enhance grip under diverse driving conditions.

To maintain air pressure in tubeless designs, a butyl-based inner liner is used to form a low-permeability barrier across the inner surface of the tire. This component eliminates the need for an inner tube and plays an important role in air retention.

In high-performance or run-flat applications, certain regions like the sidewall may include additional reinforcements or modifications to enhance load support and maintain mobility in case of pressure loss.

The construction described above reflects the tire model used in this study for finite element simulations in ABAQUS, allowing for realistic representation of the tire's structural response under dynamic conditions such as slip, camber, and inflation loss scenarios.

2.5 Need for runflat tires.

Run-flat tire (RFT) technology was developed and adopted commercially to address two primary challenges related to critical safety and mobility caused by pneumatic tires. Punctures, sidewall damages in passenger vehicles along with mines, IEDs or ballistic threats in military context often led to a rapid loss in structural integrity. Punctures coupled with slow leaks remain one of the leading causes of tire failures and often result in injuries, poor vehicle control, and sidewall collapse. Statistically, nearly 70% of highway accidents are attributed to tire punctures. The mortality rate approaches 100% when vehicles are driven on flat tires at speeds exceeding 160 km/h. Such data highlights the need for systems that preserve vehicle control in case of a blowout or deflation.

Run-flat tire design provides a solution by ensuring that the vehicles continue running even after a complete loss in inflation pressure. Self-supporting run-flat designs use reinforced sidewalls that can easily bear the vehicle load in case of deflation or a drop in internal air pressure. The sidewall uses special reinforcements which prevents it from collapsing, maintain a constant and appropriate level of ride height needed for operation and makes sure that the wheel rim remains elevated from the road surface, all while maintaining much needed handling and steering capabilities. These can allow vehicles equipped with such designs to travel safely for limited distances post-deflation, typically up to 80 km at an average speed of 80 km/hr. This provides the vehicle occupant an appropriate amount of time to exit the vehicle or reach a service point. This system is highly used in military and tactical vehicles, where mobility can be highly compromised due to tire damage. In the civilian sector, they are used in high-end luxury and sports car which often don't have enough space to carry spare tires.

One of the most important things to remember in context with run-flat tire systems is that due to reinforced construction of the sidewall, the driver may often not realise that there is a flat tire through traditional feedback mechanisms such as ride harshness or audible cues. Therefore, a tire pressure monitoring system (TPMS) is of utmost importance while implement run-flat tire design which ensures that the driver is immediately alerted when there is a change in the inflation pressure. Thus, these designs fulfill a need for reliable, damage-resistant tires that maintain vehicle mobility, safety, and continuous operations under unsafe conditions.

2.6 What is a runflat tire?

A run-flat tire (RFT) is a mutation of the conventional pneumatic tire which typically maintains vehicle mobility even after deflation. It prevents the sidewall from the collapsing

and ensures that the tire always stays attached to rim. RFTs work by preventing sudden shifts in the vehicle's centre of gravity or loss of steering control due to sudden tire pressure change. This eliminates the need for an immediate spare tire. Run-flat tires achieve functionality through internal structural reinforcements which are mostly stiffened sidewalls or support rings which can help to bear vehicle load for temporary periods of time. Some unique mechanical characteristics that RFTs possess are a higher lateral stiffness and a progressive increase in vertical stiffness, specially under increased load. This structural rigidity is highly prevalent in designs which use sidewall insert rubber (SIR).

Run flat tires were patented for the first time in 1892. However, due to technological limitations, the concept remained largely theoretical with no active commercial use. In 1934, Michelin introduced the first self-supporting tire. The design was inspired by the tires on trains and trolleys. It was built with an internal safety rim to help the vehicle to be in motion even after a loss of pressure. The tire consisted of two separate air chambers; an inner tube and an outer tube connected at the base with a small air passage. The outer tube resembled a conventional tire and the inner tube also referred to as a 'lung' consisted of two fabric layers which remained uninflated under normal conditions. Whenever the outer chamber deflated due to a blowout, the inner chamber retained air and released it gradually through a vent hole. Further advancements in 1970s and 1980s helped overcome limitations in the original design such as problems with excessive heat and increased noise. Excessive internal flexing after pressure loss caused heat buildup which was solved by adding cooling fins to the sidewalls to disperse heat and prevent structural failure. Increased noise due to stiffer sidewalls with improved material compositions and better design which almost made the difference between conventional tires and RFTs unnoticeable. These tires become quite popular as an option for sports cars during 1990s as sports car lacked the space to store spare jacks and tires. Early 2000s saw a much wider implementation of RFTs due to improve technology and more

research. BMW and Mini were the first brands to implement RFTs on a commercial scale. Although nearly twice as expensive, RFTs have become a popular choice due to safety benefits and its space-saving design.

2.7 What are the types of runflat tire?

Run-flat tires are classified into different categories based on the method used to maintain functionality after deflation. The types of RFTs popularly in use are Self-Supporting Run-Flat Tires, Auxiliary-Supported Run-Flat Tire Systems, and other emerging or hybrid concepts such as foam-filled and non-pneumatic run-flat tires.

Self-Supporting Run-Flat Tires (SSRFT)

The most prevalent type used in passenger vehicles, self-supporting RFTs have reinforced sidewalls constructed from specially formulated rubber compounds, referred to as sidewall insert rubber (SIR) which allow the tire to handle vehicle load in the absence of vehicle pressure. These reinforcements are integrated with heat-resistant cord layers and specialized bead designs to maintain rim grip under deflated conditions. The geometry and material properties of the SIR play an important role in determining the tire's mechanical behaviour.

Auxiliary-Supported Run-Flat Tire Systems

Known as support ring systems as well, this type uses an internal support ring or polymer insert mounted on the wheel rim inside the tire. In case of deflation, the vehicle load is transferred from the deflate tire directly on the ring, which then bears the contact forces with road surface. These have a higher application in military applications where extreme durability and extended mobility is needed. The ring holds the ability to roll itself along the ground in case of severe damage.

Foam-Filled Tires

Foam-filled tires are with filled with specialized foam materials to offer internal support in place of or in addition to air pressure. While not classified under conventional RFTs, foam filled designs provide puncture resistance and are used in minimal maintenance environments such as off-road applications.

Non-Pneumatic Run-Flat Tires

Zang (9) expands the definition of the run-flat capability to include non-pneumatic tires which do not use air to function. These include bionic structures, mechanically elastic wheels, or airless safety tires, offering immunity against pressure loss. Although still under research or limited commercial use, these designs represent a conceptual extension of run-flat principles.

Central Wheel-Pumping Systems

While not a structural form of the RFT, central tire inflation systems (CTIS) or automatic pressure regulation systems are considered part of the broader category of mobility-preserving tire technologies. They allow real-time pressure adjustment and re-inflation, especially useful in military and heavy-duty vehicles to counteract minor leaks or adapt to terrain.

To summarise, run-flat tire technologies cover different types of approaches that differ according to structural design, materials, and applications. The choice of RFT to implement is decided by the application type, manufacturing complexity, ride comfort and level of mobility required.

2.8 Introduction to self-supported runflat tires

Self-supporting run-flat tires (SSRFTs) are widely adopted class of RFTs which implement reinforced sidewalls that use sidewall insert rubber (SIR) that provides increased resistance to compression and bending. During deflation, the load is supported completely by the tire's internal structure such as the carcass and the reinforced sidewall eliminating the need for immediate replacement in case of blowout.

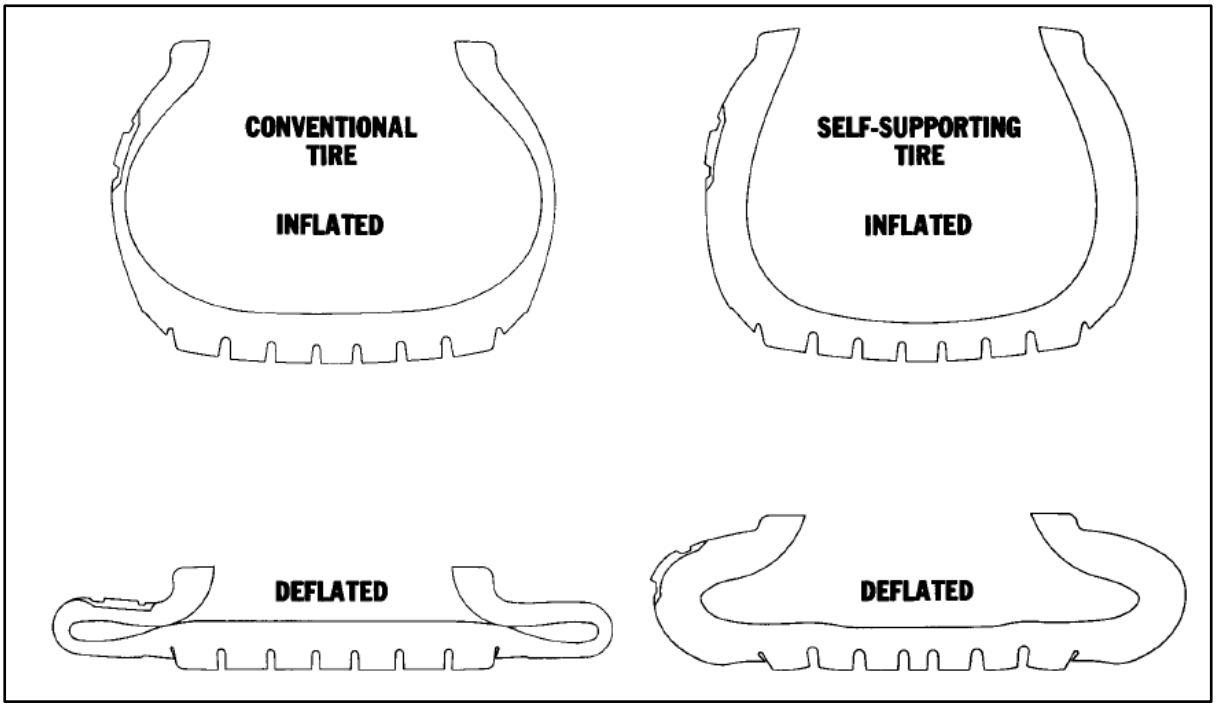

Figure 3: Inflated and uninflated cross sections of the self-supporting and conventional radial tires (10)

SSRFTs are generally rated to operate for distances up to 80 kilometres (50 miles) at speeds of up to 80 km/h (50 mph) under zero-pressure conditions, although exact capabilities vary by manufacturer and model. SSRFTs trade off the enhanced safety, reliability and convenience for higher noise levels and reduced ride comfort due to their inherently stiffer construction when compared to a conventional pneumatic tire.

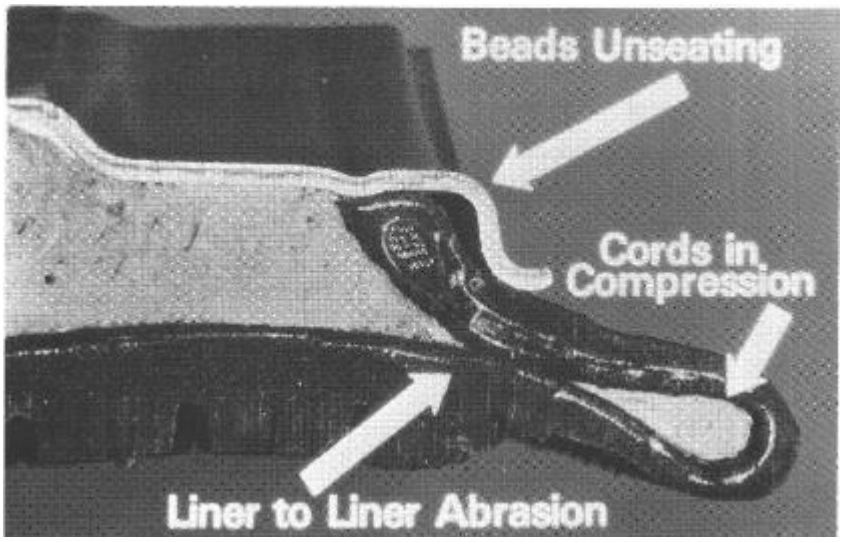

Figure 4 - Cast section of conventional tire at rated load and zero psi. (10)

The concept of self-supporting run-flat tires (SSRFTs) was first formally introduced by Alden (1977) (10), who presented a structurally reinforced radial tire designed to eliminate the need for a spare. This design incorporated load-bearing stiffness directly into the tire's sidewall using conventional materials like nylon and rayon, avoiding the complexity of insert-based systems such as polyurethane or steel rings. The final prototype demonstrated mobility beyond 45 miles at 45 MPH under deflated conditions with minimal degradation in ride quality, equivalent to a 6 PSI increase in a standard tire. Additionally, the Ridge-Loc® wheel system was developed to ensure bead retention during uninflated operation. Alden's work laid the foundation for future SSRFT designs by proving that internal reinforcement alone could maintain vehicle control and stability after deflation, without the need for significant changes to existing rims or vehicle architecture.

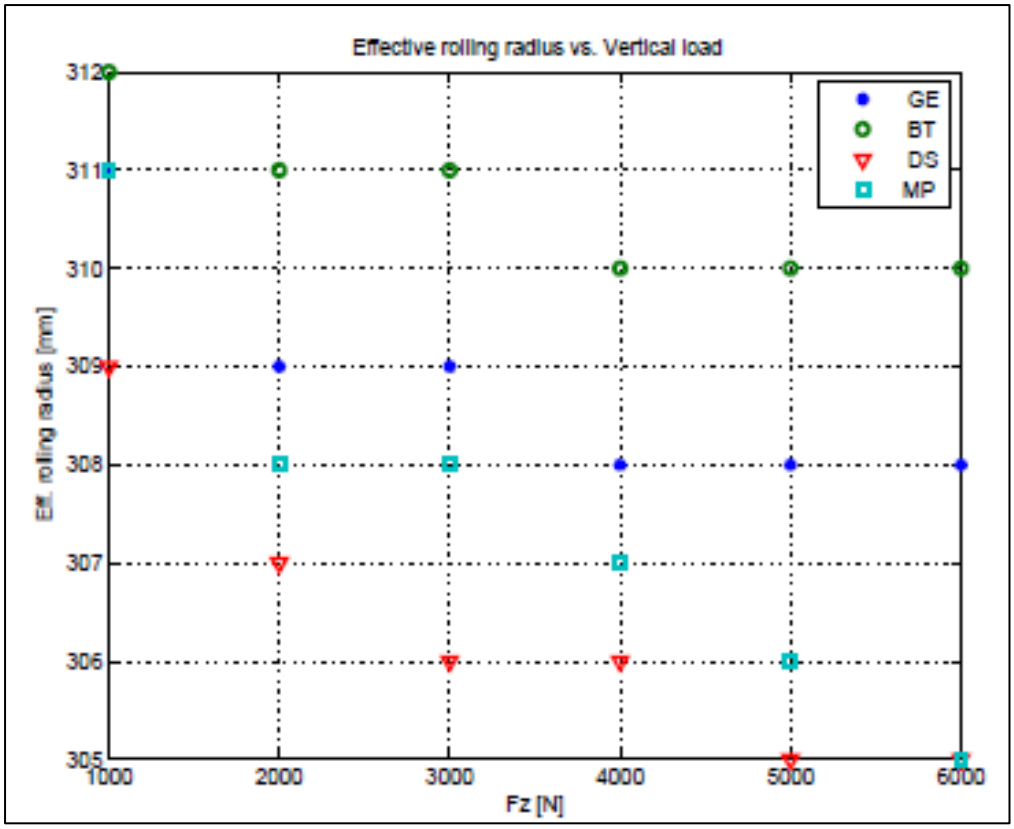

Figure 5 - Effective rolling radius. Observation of the results shows that the difference between the effective rolling radius of run flat tires and conventional tires is minimal. (11)

Veld, op het, I. B. A. (2006) (11) conducted a detailed experimental comparison between run-flat and conventional tires using a flat plank test facility, focusing on tire mechanics relevant to ride and handling. Their work analysed parameters such as effective rolling radius, vertical and lateral stiffness, sideslip relaxation, and enveloping characteristics. Results revealed that run-flat tires exhibited significantly higher lateral stiffness, by as much as 50%, as well as increasing vertical stiffness beyond 3 kN load, contributing to distinct handling behavior. Although both tire types showed similar sideslip relaxation and enveloping under vertical loads, run-flat tires produced higher vertical forces due to their reinforced structure. These findings provide an empirical foundation for understanding how structural differences in tires impact dynamic performance and were instrumental in guiding the comparative handling simulations performed in this thesis.

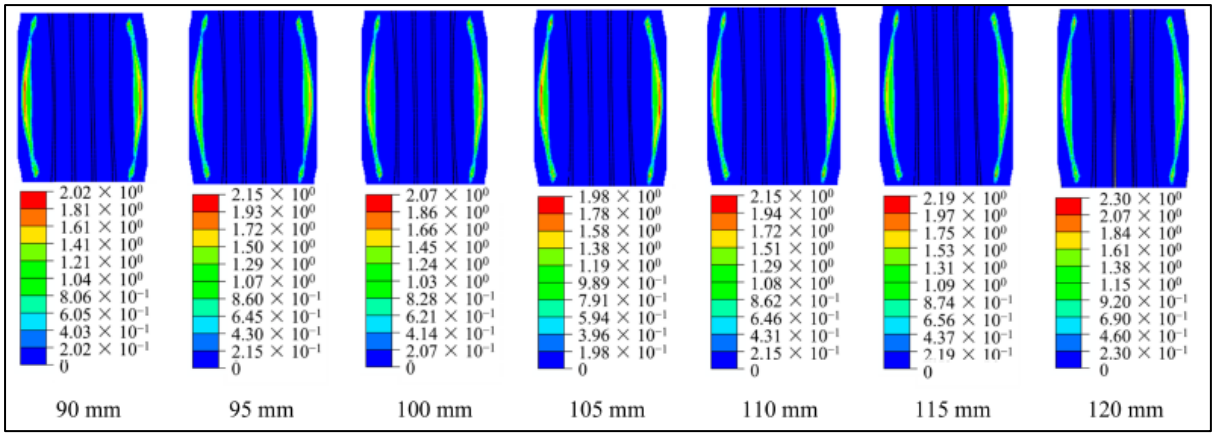

Figure 6 - Trend of tread contact stress cloud diagram with maximum width L (0 kPa) (12) .

Lv et al. (2023) (12) focused on evaluating the mechanical behavior of self-supporting run-flat tires by varying the dimensions of sidewall insert rubber (SIR), specifically insert width (L) and thickness (H). Using a validated finite element model with Yeoh hyperelastic material characterization, they demonstrated that radial stiffness increases with both L and H, with width having a more pronounced effect.

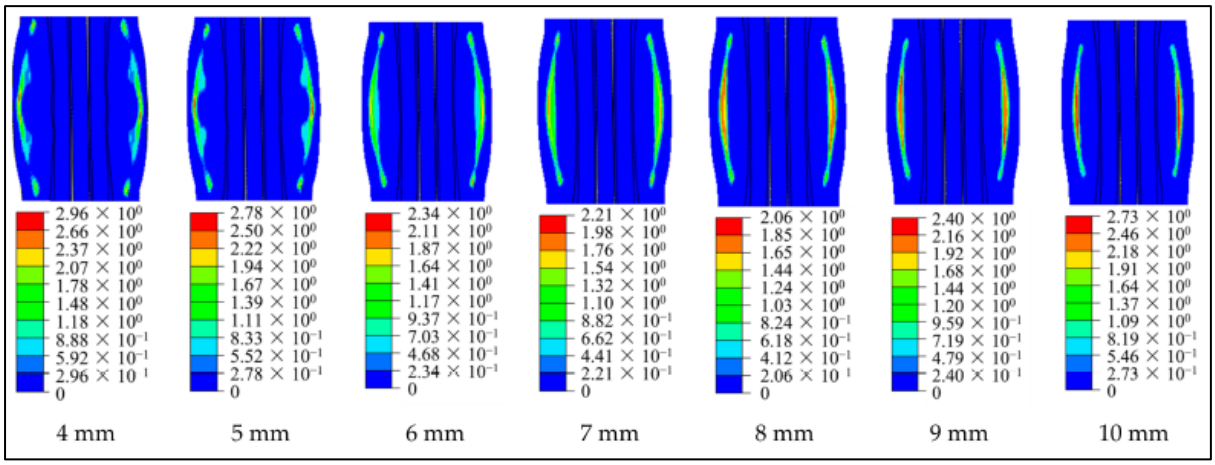

Figure 7 - Trend of tire contact stress cloud diagram with maximum thickness H (0 kPa) (12) .

Thin inserts (H < 6 mm) showed poor support and uneven stress distribution under zero-pressure conditions, while wider inserts improved structural response. Shorter widths (L < 100 mm) enhanced ride comfort under normal inflation by reducing stiffness. This study informed the material and design selection for the tire models used in this thesis and supported the understanding of trade-offs between run-flat durability and ride quality.

Cho et al. (2012) (13) proposed an optimized approach to designing run-flat tire (RFT) insert rubber using a genetic algorithm, focusing on maximizing zero-pressure performance while minimizing mass. Their study demonstrated that the geometry of the sidewall insert, especially its shape and stiffness, plays a critical role in ensuring load-bearing capability under deflated conditions. This highlights the importance of structural optimization in RFT development and provides a valuable foundation for simulation-based evaluations of tire behavior under loss of pressure.

The study by C. Venkateshwar Reddy et al. (2022) (14) investigates the structural behavior of a run-flat insert using Finite Element Analysis (FEA) under deflation and loading conditions. The paper highlights how insert thickness and material stiffness influence stress distribution and deformation, particularly under zero-pressure scenarios. These insights directly support the modelling approach used in this thesis, where sidewall reinforcement and its impact on load support are key considerations in simulating tire behavior during deflation. The study's emphasis on stress and strain tracking within the tire structure also aids in understanding force generation and stability changes post-deflation.

Arndt et al. (15) investigates the handling characteristics of vehicles equipped with temporary-use tires and self-supporting run-flat tires under various test scenarios such as circle turn and step steer (J-turn) maneuvers. It offers a comparative perspective on deflated run-flat tires versus conventional tires, specifically highlighting their influence on steer gradient, yaw rate, and spinout tendencies. Of relevance to this thesis are the observations on how deflated run-flat tires maintain greater structural support, reduce rim-ground contact, and mitigate extreme oversteer compared to standard tires under similar failure modes. The study helped shape the maneuver selection and performance metrics used in this thesis for comparing tire behavior under deflation.

Robinette and Fay (2000) (16) experimentally studied the drag and steering effects resulting from run-flat tire disablements using a 1993 Ford Taurus equipped with Michelin ZP (Zero Pressure) tires. The study involved coast-down and lateral acceleration tests to evaluate vehicle behavior under fully deflated conditions. Results showed that deflated run-flat tires produced minimal drag-induced steering and lateral deviation, with lateral accelerations typically around 0.01 g, due to the stiff sidewall maintaining tire shape. These findings provide valuable understanding of vehicle stability and control metrics, such as lateral deviation and yaw response, in post-deflation scenarios.

Heim et al. (2007) (17) investigated the impact of run-flat tire (RFT) technology on wheel design and durability, emphasizing the mechanical implications of reinforced sidewalls. Their study showed that RFTs exhibit significantly higher vertical stiffness (320 N/mm) compared to standard tires (260 N/mm), contributing to increased wheel loads during dynamic maneuvers. Experimental stress analysis revealed that RFTs induced average stress increases of 68% during straight-line driving and 56% during cornering, underscoring the need for fatigue-strength evaluation of wheels intended for use with RFTs. Using the BIAX Wheel Fatigue Test, the study further highlighted the role of tire construction in altering excitation spectra and stress distributions under transient conditions, which directly relates to tire-vehicle interactions in deflated states. These insights are essential for evaluating the structural and dynamic response of tires under pressure-loss conditions.

2.9 Construction of self-supported runflat tires

Construction of Self-Supporting Run-Flat Tires (SSRFTs)

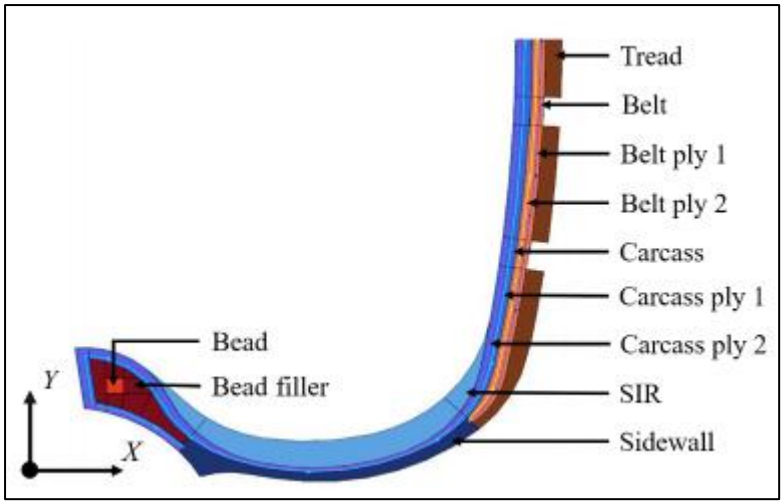

Figure 8 - Internal structure of a self-supporting runflat tire.

The key constructional features of SSRFTs are described below:

1. Reinforced Sidewall Construction

The most distinguishing feature of SSRFTs is their reinforced sidewalls. These sidewalls are designed to resist collapse and support vertical loads at zero inflation pressure. Reinforcement is primarily achieved using Sidewall Insert Rubber (SIR).

2. Sidewall Insert Rubber (SIR)

The SIR is an auxiliary structural element embedded within the sidewall. It provides compression bending resistance, which is essential in maintaining tire integrity during deflation.

Design parameters of the SIR that critically affect performance:

- Maximum width (L) – affects lateral stiffness and load distribution.
- Maximum thickness (H) – influences vertical stiffness and bending resistance.
- Geometric shape – e.g., *ladder type* or *half-moon*, which control stiffness transition behaviour.

Material properties of SIR which are key to durability and effectiveness:

- Rigidity – ensures structural support under load.
- Tensile strength – resists material failure at high strains.
- Flexion resistance – maintains integrity under repeated deflection.
- Heat generation – must be minimized as SIR experiences increased temperature during zero-pressure operation.

SIR becomes a primary load-bearing component during the final stages of pressure loss, especially when internal pressure approaches zero.

3. Specialized Beads

SSRFTs incorporate reinforced or thickened bead constructions which have two primary functions:

- Secure the tire onto the rim even when air pressure is lost.
- Prevent rim-tire separation during deflation and allow continued rolling.

This bead structure is crucial to rim retention and safe vehicle handling in a deflated state.

4. Stiffer Internal Construction

The integration of SIR and bead enhancements leads to a tire with increased lateral and vertical stiffness. This stiffer construction:

- Reduces the amount of sidewall deformation during deflation.
- Prevents the sidewall from touching the ground.
- Enables load transfer from the tread to the rim through internal structure rather than air pressure.

While improving safety and durability, this construction may result in some negative consequences such as:

- A firmer ride under normal conditions.

- Increased heat buildup during zero-pressure operation due to higher flexural energy dissipation in the sidewalls.

2.10 Finite Element Simulation Strategies for Tire analysis

The simulation of pneumatic tires using finite element methods (FEM) has become a well-established practice for analysing structural response, contact behavior, and handling-related force generation under different operating conditions. The Abaqus/Standard finite element suite provides several advanced features to conduct both static and rolling analyses, especially suited for capturing the transition from symmetric inflation to complex asymmetric deformations during cornering or deflation. This section reviews the simulation strategy as outlined in key reference examples from Abaqus, specifically focusing on methodologies that employ symmetric model generation, results transfer, and steady-state transport analysis.

2.10.1 Symmetric Modelling and Results Transfer Workflow

To reduce computational cost while retaining fidelity, Abaqus (18) provides a multi-step simulation strategy that begins with an axisymmetric analysis and evolves toward a full 3D dynamic rolling model. The sequential steps are described below:

Step 1: Axisymmetric Inflation Analysis

A 2D axisymmetric cross-section of the tire is created, exploiting reflection symmetry about the vertical plane through the wheel axis. Inflation is simulated using CGAX4H and CGAX3H elements, which support axisymmetric conditions with twist, allowing accurate circumferential stress predictions. Reinforcements such as belts and plies are embedded using rebar definitions in continuum rubber elements. A uniform internal pressure is applied to simulate tire inflation, producing the initial stress and strain distribution.

Step 2: Symmetric Model Generation and Results Transfer to Partial 3D.

The axisymmetric mesh is revolved about the central axis to create a partial 3D sector (e.g., 60°). Using Abaqus's symmetric results transfer capability, the stress and deformation state from the 2D inflation model is mapped onto this 3D sector. The partial 3D model combines C3D8H, C3D6H, and CCL12H/CCL9H elements to maintain accuracy in both curved and flat regions.

Step 3: Footprint Analysis Using Partial 3D Model.

A static footprint analysis is performed by bringing the inflated tire into contact with a rigid analytical surface (representing the road or drum). A vertical displacement is first applied to establish contact, followed by a vertical load on the rim's reference point. Friction is initially set to zero to avoid convergence issues and simplify later rolling analysis setup.

Step 4: Generation of Full 3D Model and Results Transfer

The partial 3D model is mirrored through a vertical line, accounting for skew-symmetry in belt orientation. The static results from the partial model are transferred to the full 3D mesh, establishing the initial conditions for the global deformation state. This approach is significantly more efficient than building and solving a full 3D model from scratch, offering up to 2.5× reduction in computational time.

Step 5: Equilibrium Step for Full 3D Model

A static equilibrium step is conducted to ensure that the transferred results from the partial model are in equilibrium in the full 3D configuration. Loads and boundary conditions must be redefined since they are not automatically transferred with the field data. A single increment static step with full time duration ensures a stable equilibrium initialization.

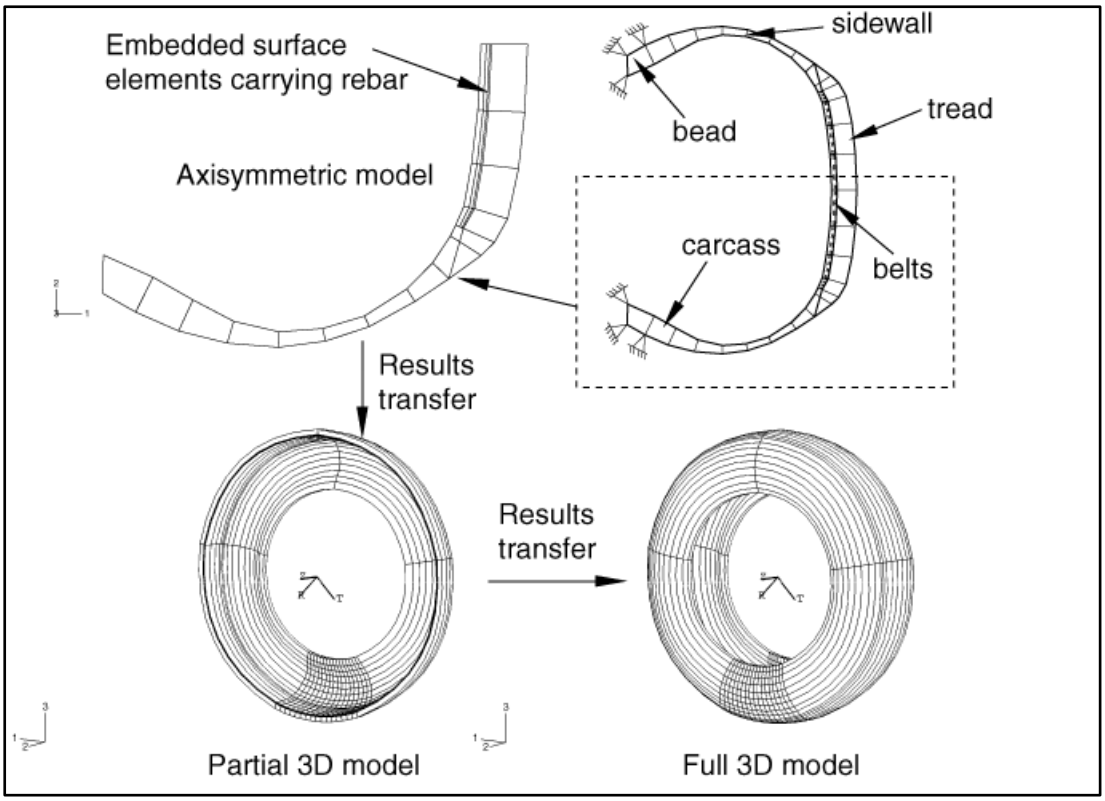

Figure 9: Symmetric Modelling and results transfer workflow.

Steady-State Rolling and Cornering Simulations

To model dynamic tire behavior such as rolling resistance, lateral force, and torque under slip, Abaqus (19) offers the steady-state transport analysis method, which is computationally more efficient than time-domain Lagrangian methods.

1. Kinematic Description

The steady-state transport method uses a mixed Eulerian-Lagrangian formulation. Material deformation is treated in a Lagrangian sense, while rigid body rotation is handled Eulerianly, enabling mesh refinement only in the contact region. The mesh is stationary in space, and tire material is “moved through” the mesh via streamlines, which are pre-computed using the revolve symmetry from static steps.

2. Model Setup and Physics

The full 3D model obtained from the static analysis is used for rolling simulations.

The model can account for, frictional contact, viscoelasticity (Prony series-based for rubber), inertia effects (neglected in low-speed simulations like 10 km/h), Viscoelastic effects are included unless a long-term or rate-independent material response is explicitly defined.

3. Simulation Process

Rolling Initialization: The analysis starts from the static footprint solution. A ground velocity is applied, and angular velocity is varied to study different rolling states. The friction coefficient is gradually ramped from 0 (used in static setup) to the desired value (e.g., 1.0), ensuring continuity.

4. Free Rolling Analysis:

The objective is to find the angular velocity at which the net torque on the rim is zero. Two simulations are performed with different angular velocities producing rim torques of opposite sign. Linear interpolation is used to find the zero-torque angular velocity, from which the free rolling radius is computed.

5. Cornering (Slip Angle) Analysis:

A slip angle is introduced by resolving the translational velocity into:

$$v_x = v.\cos(\alpha) \quad v_y = v.\sin(\alpha)$$

where V is the tire speed and α is the slip angle.

The lateral force Fy is extracted at different α values to construct lateral force vs. slip angle curves. These results are critical for parameterizing Pacejka tire models for handling simulations.

6. Camber and Drum Rolling:

Additional effects such as camber thrust and drum contact are also supported using the same framework by rotating the tire about the longitudinal axis or introducing a rotating drum surface.

7. Significance of the Strategy

This simulation logic—starting from axisymmetric inflation, progressing through partial and full 3D footprint analyses, and culminating in steady-state rolling simulations—offers a highly efficient yet accurate means of capturing key tire behaviours. The symmetric results transfer methodology provides substantial computational savings without compromising accuracy. The framework is especially effective for modelling handling characteristics in tires with asymmetric structural features, such as run-flat reinforcements, and serves as a robust foundation for deriving force-slip characteristics for use in empirical models like Pacejka's Magic Formula.

2.11 Tire Dynamics and Handling Characteristics

2.11.1 Introduction to Tire Dynamics

Tires are the primary source of force and moment generation in a vehicle and almost all key maneuvers such as acceleration, braking, and steering and are governed by interactions in the tire-road contact patch, which is often smaller than the size of a human hand. Tires fulfill three primary functions, supporting the vertical load of the vehicle, transmitting longitudinal forces for traction, and braking and generating lateral forces for cornering.

2.11.2 Tire Coordinate System and Terminology

The SAE J670 coordinate system is the standard for describing tire behavior:

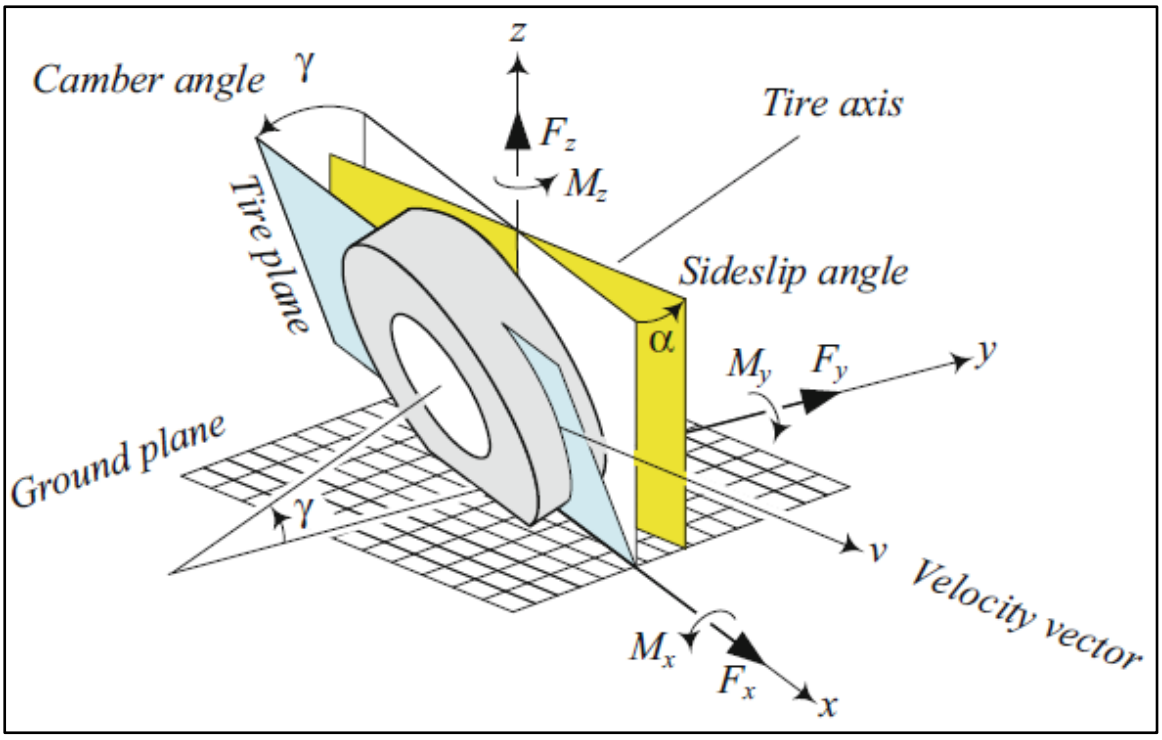

Figure 10 - Tire Coordinate System

X: Longitudinal (forward) direction.

Y: Lateral direction (to the left).

Z: Vertical direction.

The main force and moment components are:

F_x : Longitudinal force [N]

F_y : Lateral force [N]

F_z: Normal/vertical load [N]

M_x : Overturning moment (roll) [Nm]

M_y : Rolling resistance moment (pitch) [Nm]

M_z : Aligning torque (yaw) [Nm]

Key angular parameters:

Slip Angle α:

$$\alpha = \tan^{-1}(\frac{v_y}{v_x})$$

where v_x and v_y are longitudinal and lateral velocities of the tire.

Pneumatic Trail t_p Distance from contact center to the lateral force centroid.

2.11.3 Mechanics of Force and Moment Generation

Tire forces arise due to shear deformation of the tread in the contact patch. As the tire rolls, the tread elements are distorted and generate shear stresses that integrate into net forces.

Lateral Force (cornering force):

$$F_y = C_\alpha . \alpha \quad (valid\ for\ small\ slip\ angles)$$

Aligning Torque (caused by the pneumatic trail):

$M_z = F_y . t_p$

Rolling Resistance Moment: Arises from the offset in vertical load distribution due to viscoelasticity and cyclic deformation.

2.11.4 Parameters Influencing Handling Performance

Handling characteristics are sensitive to the following tire parameters:

Table 1: Key parameters sensitive to tire handling characteristics.

Parameter	Symbol	Governing equation or role
Slip angle	α	Input that governs F_y
Cornering Stiffness	C_α	$F_y = C_\alpha . \alpha \quad (valid\ for\ small\ slip\ angles)$
Aligning Moment	M_z	$M_z = F_y . t_p$
Load Sensitivity	F_z	Affects both C_α, F_y

Longitudinal Slip	κ	$\kappa = \frac{C_\alpha}{F_z}$
Cornering Coefficient	K_c	$K_c = \frac{C_\alpha}{F_z}$

2.12 Models used to study the handling performance of tires.

The accuracy of any vehicle dynamics simulation is highly dependent on the quality and fidelity of the tire model used. As the only component in direct contact with the road, the tire governs the generation of longitudinal, lateral, and aligning forces, which are fundamental to predicting vehicle handling behavior. Over the years, a wide range of tire models have been developed to cater to different simulation objectives, levels of detail, and computational requirements. Broadly, these models can be categorized into theoretical (or physical) models, empirical models, and semi-empirical models, each with varying levels of complexity and accuracy.

Theoretical or physical models attempt to represent the actual structural behavior of the tire using mechanical analogies. Classic examples include the brush model (20), which conceptualizes the tire tread as a series of elastic bristles and offers valuable physical insight into the mechanisms of force generation. Variants like the Fiala model (21) extend this framework to include lateral force saturation and basic aligning moment behavior. More advanced physical models such as the flexible ring model (21) and finite element (FE) models incorporate detailed representations of carcass and tread deformation, making them capable of simulating high-fidelity tire-road interaction. However, the computational cost of such models often restricts their use to tire design or low-speed transient analyses rather than full-vehicle dynamic simulations.

Semi-empirical models integrate measured data while embedding structural features or assumptions derived from physical models. These models aim to balance the empirical accuracy of data fitting with physically interpretable parameters. For example, Gim's semi-physical model (21) has been applied successfully to both handling and braking simulations. While these models offer improved realism over purely empirical models, they typically require more extensive parameter identification and may not generalize easily across different operating conditions.

Empirical models, in contrast, are purely data-driven and derive force and moment outputs through curve fitting to experimental tire test data. These models prioritize predictive accuracy for a specific dataset over physical interpretability. Among them, the Magic Formula, also known as the Pacejka model (20), is the most widely adopted for vehicle handling and stability analysis. It provides closed-form expressions for lateral force, longitudinal force, and aligning moment as nonlinear functions of slip angle, slip ratio, normal load, and camber angle. The general lateral force form of the Magic Formula is expressed as:

$$F_y(\alpha) = D.\sin\left(C.\tan^{-1}\left(B.\alpha - E\left(B.\alpha - \tan^{-1}(B.\alpha)\right)\right)\right)$$

where:

B is the stiffness factor,

C is the shape factor,

D is the peak factor,

E is the curvature factor,

α is the slip angle.

The Magic Formula is highly flexible and can be extended to account for combined slip, camber effects, turn slip, and tire asymmetries such as conicity and ply steer. Its major advantage lies in its ability to closely replicate real tire behavior over a wide range of operating conditions using a relatively small set of parameters. This makes it highly suitable for use in both offline simulations and real-time control system development environments.

For the purposes of this thesis - which focuses on evaluating the handling performance differences between self-supporting run-flat tires and conventional tires - the Magic Formula offers a practical and validated approach. It provides an appropriate balance of accuracy, empirical fidelity, and computational efficiency. Moreover, it allows for the effective characterization of tire lateral and longitudinal behaviours under steady-state and quasi-steady-state slip conditions, which are central to the study of vehicle handling. Accordingly, the Pacejka Magic Formula is adopted in this work as the primary tire force model and forms the foundation for all vehicle dynamic simulations carried out in this thesis.

3. Finite element modelling of tires.

3.1 Structural Simulation Methodology

To simulate the deformation, loading response, and handling performance of both standard and self-supporting run-flat tires (SSRFTs), a multi-phase finite element modelling strategy was implemented in Abaqus/Standard. The work builds upon validated methodology as shown in Abaqus Examples (18) (19) but incorporates customized element types, contact definitions, and load paths tailored to investigate both inflated and deflated tire states under realistic conditions.

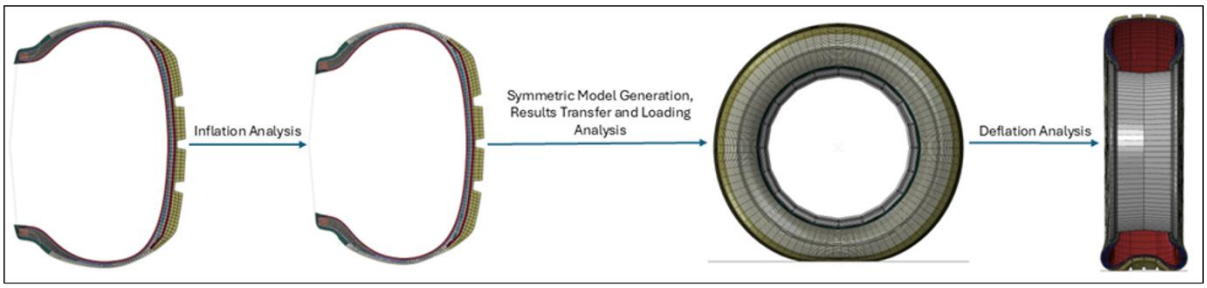

Figure 11- Overview of the sequential simulation process, including 2D axisymmetric inflation, 3D revolved model generation, loading and deflation.

Figure 11 illustrates the overall simulation methodology adopted in this study. The finite element modelling approach began with a 2D axisymmetric inflation analysis to establish the pressurized tire configuration. The inflated configuration was then revolved to form a full 3D model for vertical loading and contact analysis. This intermediate state served as the starting point for simulating partial or complete deflation. Finally, the deflated geometry was used in steady-state rolling and cornering simulations, enabling detailed assessment of lateral deformation, contact pressure, and structural response across different inflation states. This multi-step strategy ensured consistent transfer of field variables and minimized computational cost while preserving mechanical fidelity.

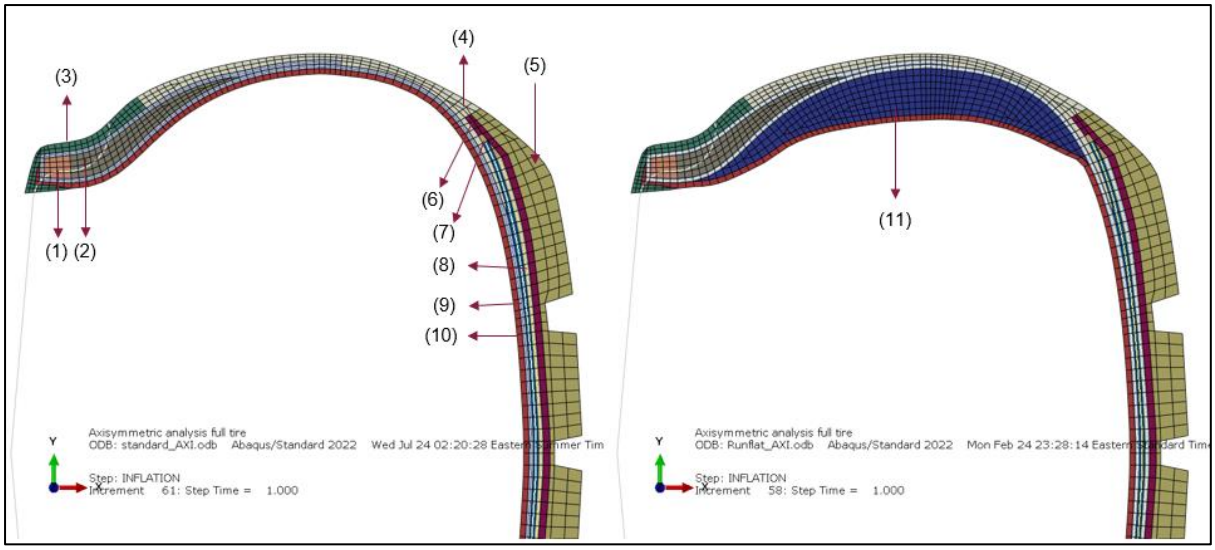

Figure 12- Tire model mesh and components.

The modelling of tires begins with a 2D axisymmetric layout, where each section of the tire is represented as a distinct region corresponding to different rubber components and reinforcements. Figure 12 illustrates the various components modelled in this study. These sections are described as follows:

1. Bead - Anchors the tire to the rim and provides structural rigidity at the base.
2. Bead Filler/Apex - A stiff rubber compound above the bead, enhancing ride stability and cornering performance.
3. Rim Strip - A protective layer between the rim and the tire structure, preventing mechanical damage.
4. Sidewall - The outermost layer of the tire's side, providing flexibility and protection.
5. Tread - The contact surface with the road, designed for grip and wear resistance.
6. Tread Base - A cushion layer beneath the tread that helps in distributing stresses.
7. Belt Edge - The boundary area of the reinforcement belts, helping control deformation.
8. Belt Edge and Belt Gum - Provides bonding and damping between belts and surrounding rubber.

9. Ply and Ply Gum - Main reinforcing layers that carry loads and maintain the shape of the tire.
10. Inner Liner - An airtight layer that retains internal pressure.
11. Sidewall Insert (Reinforcement) - Additional structural support within the sidewall to improve lateral stiffness and durability.

3.1.2 Axisymmetric Inflation Model

The modelling process began with a 2D axisymmetric cross-section of the tire using CGAX3H and CGAX4H hybrid elements to represent rubber components. Key reinforcement layers, such as belts and plies, were embedded using rebar layers defined within surface sections. These reinforcements were oriented at defined angles (e.g., ±68° for belts) to reflect actual ply architecture. A uniform internal pressure of 250 kPa was applied to simulate inflation. Rim mounting was achieved through displacement boundary conditions applied to nodes representing bead seats.

Figure 13 illustrates the inflation process, in the left plot, the tire is undeformed with zero internal pressure, showing no contact between the bead region and the rim. In the right plot, following the application of 250 kPa internal pressure, the tire inflates and deforms outward, establishing uniform contact with the rim as indicated by the CPRESS distribution. This

confirms successful rim mounting driven purely by inflation pressure.

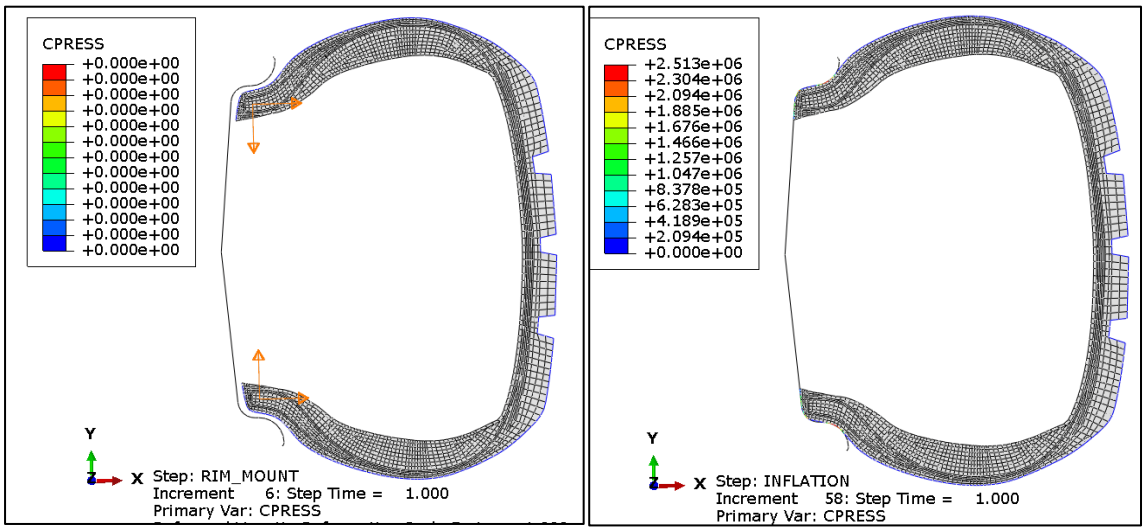

Figure 13: 2D axisymmetric cross-section of the tire showing contact pressure (CPRESS) distribution before inflation (left, post rim-mounting) and after inflation (right) under 250 kPa internal pressure.

3.1.3 Transition to Partial 3D Sector

The inflated 2D mesh was revolved into a 90° symmetric 3D sector using the *SYMMETRIC MODEL GENERATION* capability. Rebar layers were transferred to solid elements using embedded element definitions, and reinforcement mapping was applied via SFMGAX1-to-SFM3D4R transformation. The inflation results from the 2D step were transferred into the 3D domain using *SYMMETRIC RESULTS TRANSFER*, enabling continuity in stress-strain initialization.

3.1.4 Vertical Loading and Contact Setup

Vertical loading was applied to the tire through a two-step analysis: an initial displacement-controlled rim motion, followed by a vertical force of 4905 N applied at the rim node. Contact with the road was modelled using a rigid analytical surface and a zero-friction setup during initial footprint seating. Frictional behavior was subsequently enabled using *CHANGE FRICTION* to simulate realistic interaction with the rim and ground.

3.1.5 Deflation Simulation

To model deflation in SSRFTs, the internal pressure was reduced from 250 kPa to 130 kPa in a stabilized static step. This was performed while maintaining vertical load to ensure structural realism and avoid convergence issues associated with collapsing geometries. Contact stabilization and soft constraints were introduced to handle potential wrinkling or loss of stiffness in the deflated tire sidewall.

3.1.6 Contact Patch and Structural Deformation Comparison

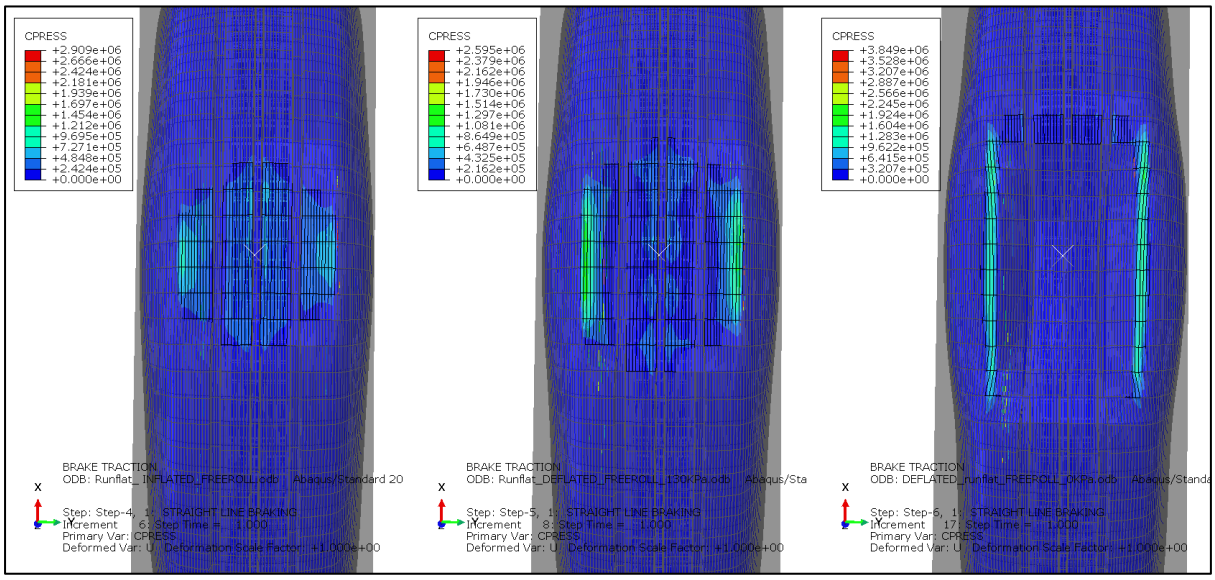

Figure 14 - Contact Patch plot for runflat tire; inflated (left), deflated 130 kPa (middle), deflated 0 kPa (right).

To evaluate the impact of internal pressure variation on tire-road contact characteristics, the steady-state rolling simulation results were post-processed to extract contact pressure (CPRESS) distributions and structural deformation states under three conditions: fully inflated (250 kPa), partially deflated (130 kPa), and fully deflated (0 kPa). Figure 14 shows the top-view contact patch distributions, where it can be observed that deflation causes the contact area to elongate along the lateral edges, shifting the peak pressures outward from the center.

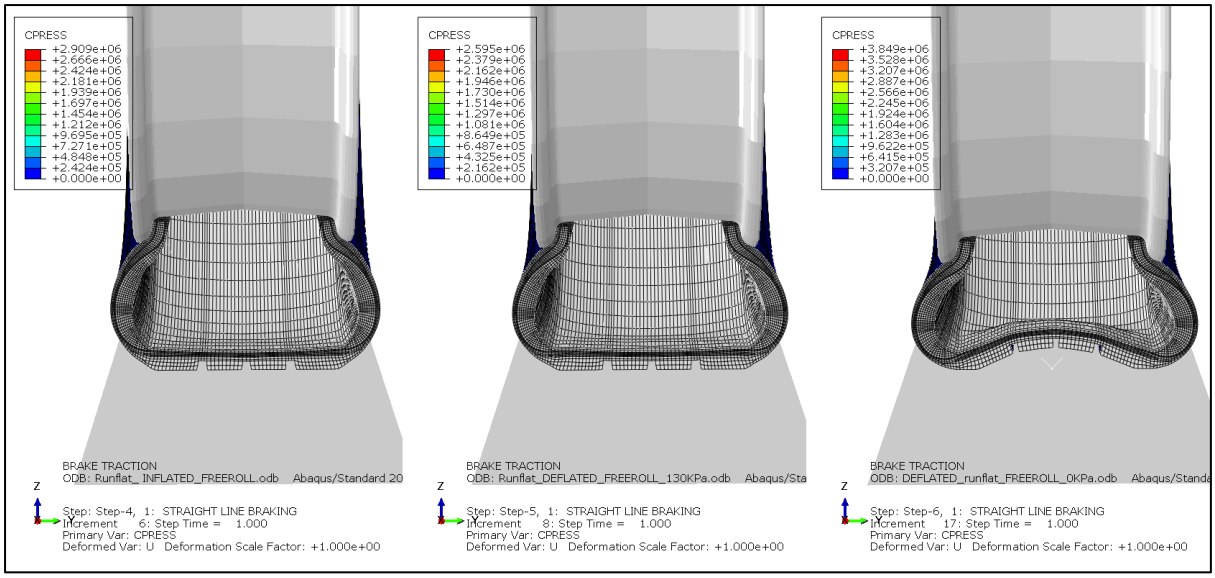

Figure 15 - Cross-sectional deformation plot for runflat tire: inflated (left), deflated 130 kPa (middle), deflated 0 kPa (right).

Complementing this, Figure 15 presents cross-sectional views of the tire deformation under the same loading and rolling conditions. These cut-section plots highlight the increasing collapse of the sidewall structure as pressure decreases, especially at 0 kPa, where the sidewall insert significantly flattens to carry the load. These visualizations reinforce the importance of sidewall structural stiffness and contact footprint uniformity in maintaining ride stability during run-flat operation.

3.1.7 Steady-State Rolling and Slip Angle Definition

The final phase consisted of a sequence of steady-state transport steps to simulate rolling and cornering conditions. A full 3D model with the previously computed field variables was used. The tire was assigned a ground velocity and rotational velocity based on an initial free-rolling solution. Cornering behavior was simulated by resolving the tire's translational velocity into longitudinal and lateral components corresponding to slip angles of 1°, 2°, 3°, and 4°. The appropriate velocity components were prescribed directly using *MOTION, TYPE=VELOCITY* and *TRANSPORT VELOCITY* definitions. Each step yielded steady-state lateral force values, which were used to construct the lateral force–slip angle curves essential

for Pacejka model parameterization.

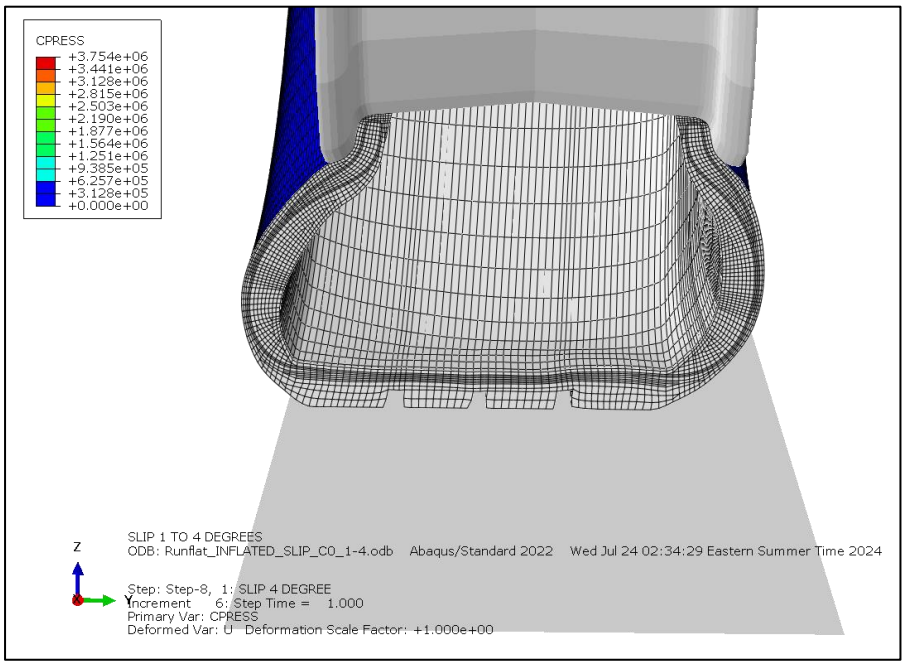

Figure 16 - Cut-section view of inflated run-flat tire under 4° slip angle, showing moderate lateral deformation and intact sidewall structure.

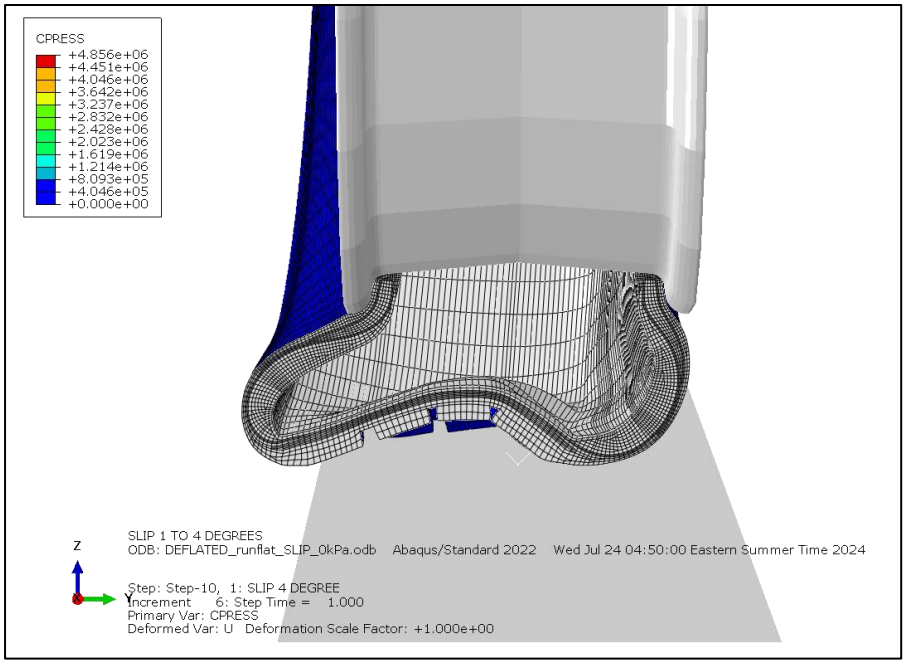

Figure 17 - Cut-section view of deflated (0 kPa) run-flat tire under 4° slip angle, highlighting significant sidewall collapse and inward deflection to sustain lateral loading.

During steady-state rolling simulations at a slip angle of 4°, noticeable differences emerge between inflated and fully deflated (0 kPa) run-flat tire conditions. As illustrated in Figure 16, the inflated tire maintains its sidewall geometry with moderate lateral deformation,

supporting the structure effectively under cornering load. In contrast, Figure 17 reveals that the deflated configuration leads to substantial sidewall collapse and inward deformation, as the insert takes on the load-bearing role in the absence of internal pressure.

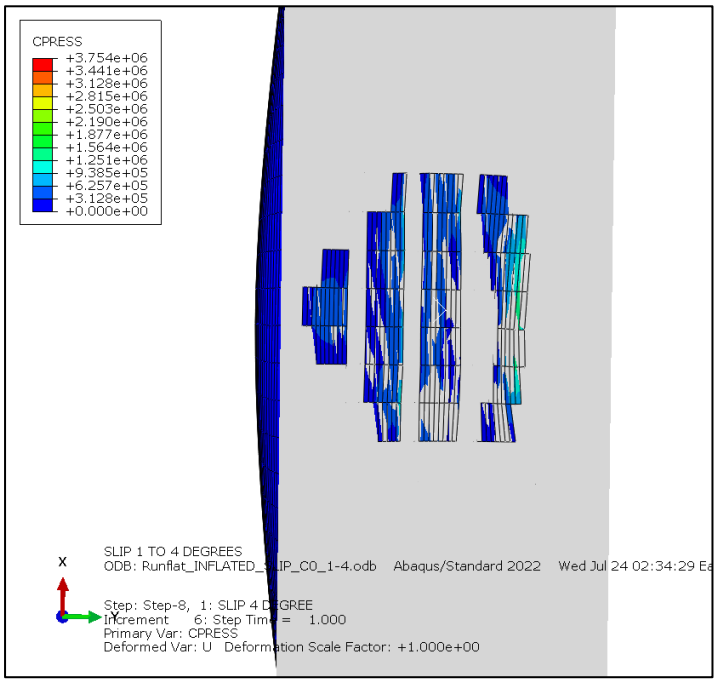

Figure 18 - Contact pressure distribution for inflated run-flat tire at 4° slip angle, showing a stable elliptical footprint with uniform load spread.

Contact pressure distributions further emphasize this contrast. Figure 18 shows the inflated run-flat tire exhibiting a uniform and centered footprint with stable pressure spread across the contact patch. Meanwhile, Figure 19 demonstrates how deflation results in a narrower and laterally shifted contact zone, reflecting compromised pressure support, and highlighting the importance of sidewall integrity for maintaining footprint shape during slip-induced cornering.

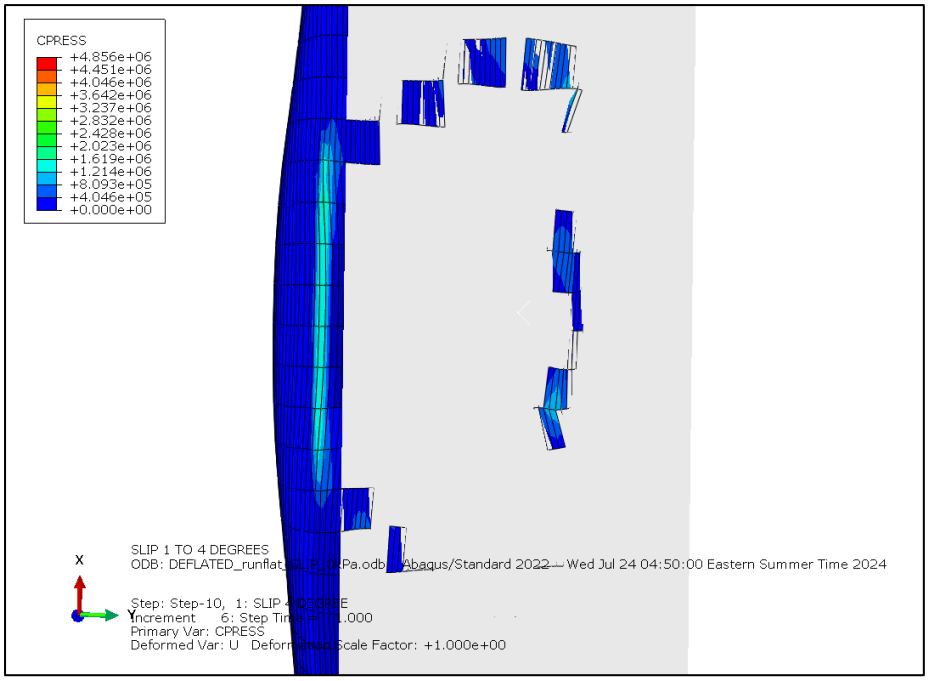

Figure 19 - Contact pressure distribution for deflated (0 kPa) run-flat tire at 4° slip angle, illustrating a narrowed and shifted footprint due to altered structural support.

3.1.8 Remarks on Implementation

All modelling steps were executed using a fully 3D configuration to accurately capture asymmetric deformation during deflation. The decision to use a full model over a mirrored half was critical in enabling realistic simulation of sidewall collapse in SSRFTs. Additionally, care was taken to apply deflation after vertical loading, as this sequence improved numerical stability and aligned with physical loading procedures. The simulation framework produced not only accurate contact patch evolution and radial deformation patterns, but also provided high-fidelity inputs for empirical tire model fitting and dynamic vehicle simulation.

3.2 Tire dimensions, boundary and loading conditions.

The tire modelled in this study is a self-supporting run-flat (SSR) radial tire with size specification 175/70 R14, a standard profile used in passenger vehicles. The tire is mounted on a 5Jx14 steel rim, consistent with OEM mounting for the selected profile. The internal construction of the tire includes all primary structural components such as tread, sidewalls, inner liner, carcass plies, steel belts, bead fillers, and reinforcing inserts. These geometric

features were inherited from validated tire data and were implemented with sufficient fidelity to replicate realistic stiffness and deformation behavior. The full geometry was modelled as a 3D solid to enable analysis of asymmetric deflections, particularly under run-flat conditions.

3.2.1 Material Properties and Constitutive Behavior

Material definitions for the tire were selected based on literature-calibrated datasets and standard industry sources. The rubber matrix was defined using incompressible hyperelastic models, while the reinforcement layers (belts and plies) used linear elastic definitions to capture the behavior of embedded cords. High-modulus materials were assigned to beads to mimic the performance of bundled steel wires. Additionally, Prony series-based viscoelasticity was applied to selected rubber compounds to reflect time-dependent behavior under rolling loads, particularly in the contact patch region.

3.2.2 Loading Conditions and Inflation States

To replicate realistic loading, the tire was subjected to a static vertical load of 500 kg, simulating one-fourth of the total vehicle weight for a gross mass of 2000 kg. This load was applied at the rim center during the footprint and deflation stages. Two inflation scenarios were defined: 250 kPa representing the nominal inflated state and 130 kPa representing a partially deflated run-flat condition. These values were selected to study the comparative structural response and lateral force generation of the tire under different inflation pressures.

3.2.3 Rolling and Cornering Assumptions

The tire was analysed under steady-state rolling conditions using a fixed mesh Eulerian-Lagrangian formulation. The rolling velocity was set to 20.11 m/s (equivalent to 45 mph), a common benchmark for handling evaluation. The road surface was modelled as an analytical rigid body with a friction coefficient of 0.8, representative of dry asphalt. To simulate cornering, slip angles from 0° to 4° were imposed by decomposing the tire's translational

velocity vector into lateral and longitudinal components. The tire was allowed to rotate freely under the applied motion, with no external torque applied at the rim, enabling natural rolling dynamics.

3.2.4 Boundary and Initial Conditions

All simulations were initialized from a static footprint equilibrium state obtained through symmetric results transfer. This ensured consistent internal stress and strain conditions across both inflated and deflated simulations. Boundary conditions were defined to restrict rigid body motion without artificially influencing the tire's deformation or force response. This setup allowed for accurate evaluation of both structural integrity and handling capability across inflation states, providing the basis for comparison between standard and run-flat tire configurations.

4. Tire modelling

4.1 Force and Moment Data Extraction

Simulation outputs included the following quantities: Lateral force (F_y), Longitudinal force (F_x), Aligning moment (M_z). For the purposes of vehicle lateral dynamics simulation, primary emphasis was placed on lateral force (F_y) as a function of slip angle. Forces were extracted at the tire hub reference point, ensuring consistency in sign conventions. The extracted force-slip data as seen in Figure 20 was organized in an Excel spreadsheet structure for post-processing.

Camber (°)	Slip Angle (°)	Longitudinal Slip (%)	RF1 (N)	RF2 (N)	RF3 (N)	RM1 (Nm)	RM2 (Nm)	RM3 (Nm)
0	0	0	17.1001	-210.5	4906.74	-60.5504	-0.177894	9.90046
0	**1**	0	34.86120224	1427.281738	4906.74	402.1270142	-7.761754036	-36.2967186
0	**2**	0	-51.97058487	2467.04834	4906.74	696.2555542	18.21363258	-41.95172882
0	**3**	0	-75.82624817	2980.296143	4906.74	843.6303101	25.67409897	-34.33693695
0	**4**	0	-111.6343994	3326.408203	4906.74	943.9910278	35.62940979	-26.16852379
0	**5**	0	-153.7071228	3554.395264	4906.74	1010.513794	46.89826965	-18.60422134
0	**6**	0	-191.5816498	3710.062988	4906.74	1056.09375	56.8330574	-12.46027374
0	**7**	0	-217.547287	3810.612549	4906.74	1085.512329	63.43342972	-8.363273621
0	**8**	0	-244.6792297	3856.75415	4906.74	1099.103027	70.75770569	-6.072456837
2	1	0	18.7572937	1407.618652	4906.74	447.7959595	-3.877321482	-26.98299408
2	2	0	-99.38407135	2519.211182	4906.74	761.4685669	30.43181801	-32.79531479
2	3	0	-115.2470703	2978.888672	4906.74	892.4354248	35.00551224	-24.98056221
2	4	0	-141.6650391	3257.836426	4906.74	972.5911255	42.1493721	-17.73136139
2	5	0	-167.7369995	3446.508301	4906.74	1027.070679	48.84123993	-12.02587605
4	1	0	-5.079850674	1512.619995	4906.74	528.661438	2.487374544	-17.57446289
4	2	0	-84.61469269	2411.496094	4906.74	780.9788208	24.27202988	-25.42863274
4	3	0	-127.0667343	2896.630127	4906.74	918.0610962	36.90855408	-17.88521576
4	4	0	-150.3556519	3141.436035	4906.74	987.8643188	43.30144501	-11.2320385
4	5	0	-165.4352264	3269.843994	4906.74	1024.814453	47.01220322	-7.804973125
5	1	0	10.42765331	1565.969482	4906.74	566.9550171	-2.582655907	-12.9256134
5	2	0	-88.28347778	2407.840576	4906.74	804.4033203	25.30086899	-20.70451546
5	3	0	-116.0688629	2820.843018	4906.74	921.3266602	32.81526947	-15.48077488
5	4	0	-138.2681122	3055.484619	4906.74	987.8809814	38.66477585	-9.603170395
5	5	0	-162.0990753	3165.069336	4906.74	1019.060486	45.05435181	-6.683211327

Figure 20 - Sample of Extracted Force and Moment Data from Finite Element Simulation (Runflat Inflated Tire)

Lateral force values at each slip angle increment were recorded separately for: Standard Inflated Tire, Standard Deflated Tire, Runflat Inflated Tire, Runflat Deflated Tire

4.2 Pacejka Model Fitting Procedure

The empirical Pacejka Magic Formula was used to fit the lateral force vs slip angle data for each tire configuration:

$$F_y(\alpha) = D.\sin\left(C.\tan^{-1}\ \left(B(\alpha - S_x)(1-E) + E.\tan^{-1}\left(B(\alpha - S_x)\right)\right)\right) + S_y$$

where:

B: stiffness factor

C: shape factor

D: peak factor

E: curvature factor

Sx, Sy: horizontal and vertical shifts

The fitting was performed in MATLAB using the *lsqcurvefit* optimization function. Initial parameter guesses were based on known characteristics:

D approximated from peak lateral force.

C assumed near 1.5–2.0 initially.

B tuned for appropriate initial slope (cornering stiffness).

E adjusted to control the drop-off after peak.

The fitted coefficients for each tire case are summarized in Table 2 and the respective fitted curves are shown in Figure 4.

Table 2: Final Fitted Pacejka Coefficients.

Tire Type	B	C	D	E
Standard Inflated	11.8706	1.9289	3577.5	0.4501
Standard Deflated	17.3910	0.8000	4919.8	0.5034
Runflat Inflated	20.0890	1.0688	4162.9	0.5548
Runflat Deflated	17.4367	0.8001	4769.7	0.6061

Each fitted curve is plotted in Figure 21 against the original FEA data for visual validation. The red curves represent the fitted Magic Formula outputs, while black dots denote raw simulation points. Notably standard deflated shows early saturation and sharp drop-off, indicating abrupt lateral force loss. Runflat deflated exhibits a higher peak force and a more progressive force curve, suggesting superior cornering retention during failure.

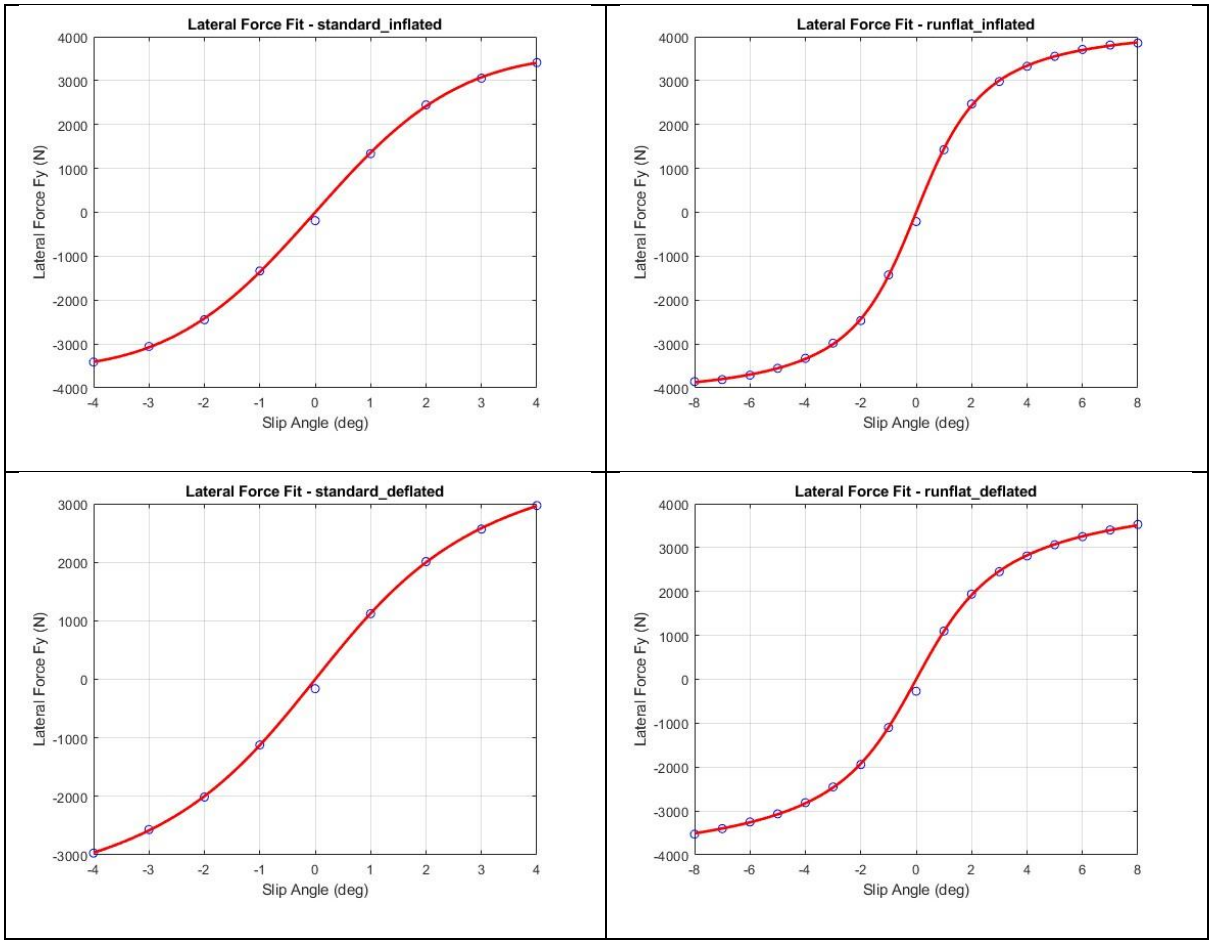

Figure 21: Lateral force vs. slip angle comparison for standard and run-flat tires under inflated and deflated conditions. The red lines represent fitted curves using the Magic Formula, while the circular markers denote simulation data. Run-flat tires exhibit higher lateral force capacity and a more gradual saturation behavior compared to standard tires, particularly under deflated conditions.

5. Vehicle Model and Stability Controller Design

This chapter presents the formulation of the full vehicle dynamics model used to assess the performance of standard and run-flat tires under varying inflation conditions. A double-track four-wheel model was adopted for this study to accurately represent the asymmetries in tire forces that arise during deflation, especially for self-supporting run-flat tires. This model accounts for individual left and right wheel dynamics at both the front and rear axles, enabling detailed analysis of lateral and yaw behavior under transient maneuvers. The model was implemented in MATLAB and incorporates the semi-empirical tire forces generated using the Pacejka Magic Formula, as described in Chapter 3. A velocity-scaled proportional controller was implemented to enable automatic path-following during steering maneuvers.

5.1 Vehicle Model Formulation

The vehicle is modelled using a nonlinear double-track representation, also known as a four-wheel planar bicycle model. Each of the four tires, front-left (FL), front-right (FR), rear-left (RL), and rear-right (RR), is modelled independently, allowing simulation of differential slip angles and lateral force generation.

Assumptions:

- Planar vehicle motion: roll, pitch, and vertical (z) dynamics are not modelled explicitly.
- Constant longitudinal velocity v_x is assumed. Steering input is applied only at the front axle (Ackermann steering not considered).
- No longitudinal acceleration or braking torque is included.
- Suspension effects are not modelled dynamically, but lateral load transfer is captured via a quasi-static approximation.

- Road is flat and uniform with no banking or elevation.
- Aerodynamic and environmental forces are neglected.

These assumptions align with standard modelling practices in mid-fidelity vehicle dynamics models (22).

5.1.2 State Variables and Equations of Motion

The state vector of the vehicle is:

$$x = [v_y \quad r \quad x_g \quad y_g \quad \psi]^T$$

The state variables of the system include the lateral velocity v_y, yaw rate r, global positions of the CG x_g, y_g, and the yaw angle ψ, assuming a constant longitudinal velocity V_x.

$$\dot{v_y} = \frac{(F_{yFL} + F_{yFR} + F_{yRL} + F_{yRR})}{m} - v_x . r$$

$$\dot{r} = \frac{L_f . (F_{yFL} + F_{yFR}) - L_r (F_{yRL} + F_{yRR}) + \frac{t_f}{2}(F_{yFR} - F_{yFL}) + \frac{t_r}{2}(F_{yRR} - F_{yRL})}{I_z}$$

$$\dot{x_g} = v_x \cos(\psi) - v_y \sin(\psi)$$

$$\dot{y_g} = v_x \sin(\psi) - v_y \cos(\psi)$$

$$\dot{\psi} = r$$

Where:

$F_{y,i,j}$: lateral tire force at wheel position from the Magic Formula

m: vehicle mass

I_z : yaw moment of inertia

L_f, L_r : distances from CG to front/rear axle.

t_r, t_f : front and rear track widths

v_x : constant longitudinal velocity

x, y: global position of vehicle CG

5.1.3 Tire Force Modelling with Magic Formula

Each tire's lateral force is computed using the Pacejka "Magic Formula"**,** a widely used semi-empirical tire model (23). It is fitted to both inflated and deflated conditions from finite element (FE) simulation data. The lateral force F_y is computed as:

$$F_y(\alpha, F_z) = \left(\frac{F_z}{F_{z0}}\right).[S_y + D.\sin\left(C.\tan^{-1}(B(\alpha - S_x)(1-E) + E.\tan^{-1}(B(\alpha - S_x)))\right)]$$

Where:

α: $slip\ angle\ at\ the\ tire$

$F_z = current\ vertical\ load\ on\ the\ tire$

$F_{z0} = nominal\ load\ (used\ for\ scaling)$

B, C, D, E, S_x, S_y: $Pacejka\ coefficients\ (different\ for\ inflated\ and\ deflated)$

The slip angles for individual tires are computed as:

$$\alpha_{FL} = \delta - \frac{v_y + L_{fr} + t_{\frac{f}{2}}r}{V_x} \qquad \alpha_{FR} = \delta - \frac{v_y + L_f r + t_{\frac{f}{2}}r}{V_x}$$

$$\alpha_{RL} = -\frac{v_y - L_r r + t_{\frac{r}{2}}r}{V_x} \qquad \alpha_{RR} = -\frac{v_y - L_f r + t_{\frac{r}{2}}r}{V_x}$$

Each tire receives its respective tire model function (Fy_FL, Fy_FR, etc.) based on the inflation condition at runtime.

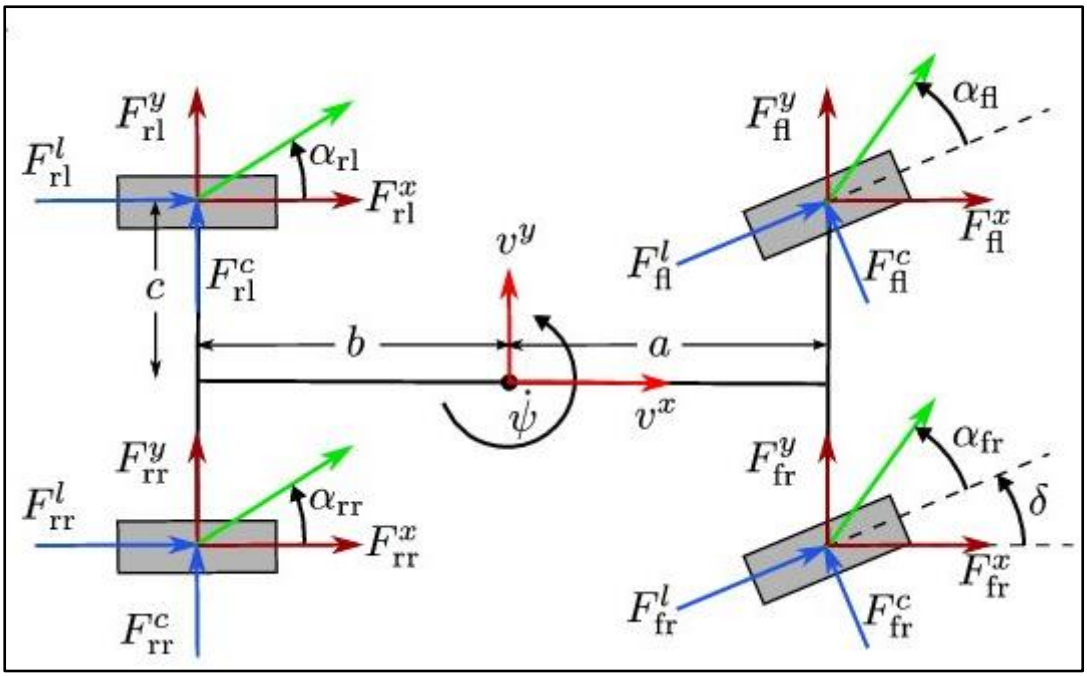

Figure 22: Schematic of the double-track model showing CG, tire forces, yaw moment arms, and slip angles for all wheels also accounting for lateral load transfer due to cornering.

5.1.4 Lateral Load Transfer

To improve model fidelity under transient steering, the normal load at each tire is dynamically updated using quasi-static lateral weight transfer. This method estimates load shifts across the vehicle track using lateral acceleration and the CG height. This method is common in handling models where full roll dynamics are omitted but load effects are still desired (22).

The lateral acceleration is:

$$a_y = \dot{v}_y + V_x r$$

Load transfer per axle is:

$$\Delta F_{z,f} = \frac{m a_y h_{CG} L_r}{(L_f + L_r) t_f}, \quad \Delta F_{z,r} = \frac{m a_y h_{CG} L_f}{(L_f + L_r) t_r}$$

Resulting tire normal forces are:

$$F_{z,FL} = F_{z0} - \Delta F_{z,f} \qquad F_{z,FR} = F_{z0} - \Delta F_{z,f}$$

$$F_{z,RL} = F_{z0} - \Delta F_{z,r} \qquad F_{z,RR} = F_{z0} - \Delta F_{z,r}$$

5.1.5 Vehicle Parameters

The parameters used for the simulation are based on a mid-size passenger car:

m = 1500 kg

I = 2250 kg·m²

Lf = 1.2 m

Lr = 1.6 m

Vx = 14 m/s (unless otherwise specified)

t_f = t_r = 1.6 m

h_cg = 0.55 m

These parameters remain fixed throughout all simulations for consistency in comparison across tire models and maneuvers.

5.2 Path-Following Control Law

To ensure the vehicle follows a predefined trajectory during simulation, a closed-loop feedback steering controller was implemented. The goal of the controller is to minimize both the lateral position error and the heading angle error of the vehicle relative to the reference path. The control law used was a composite of feedforward and feedback components:

$$\delta = \delta_{ff} - K_y . y_e - K_\psi . \psi_e - K_i \int y_e dt$$

Where:

δ is the commanded steering angle

$\delta_{ff} = \frac{L_f + L_r}{R_{ref}}$ is the feedforward steering angle for a circular path.

y_e is the lateral deviation of the vehicle from the reference path.

ψ_e is the heading angle error.

$K_y, K_\psi, and\ K_i$ are the proportional and integral control gains respectively.

This control law is executed at each time step using current state estimates (y, ψ) and their respective reference values. An integral term was included to reduce steady-state lateral error, with an integrator clamping mechanism to avoid windup when the steering command exceeds physical constraints. The steering angle is limited within a saturation range:

$$\psi \in [-0.4, +0.4]\ radians$$

The feedforward term δ_{ff}enables proactive curvature tracking for constant-radius paths, while the feedback terms ensure corrective action based on actual deviation from the path. The complete controller logic was implemented in MATLAB, integrated with the full vehicle model that accounts for slip angles, tire forces via the Magic Formula, and dynamic load transfer. The lateral and heading errors are computed based on the deviation from the dynamically computed reference trajectory.

Control gains used: $K_y = 0.03 \mid K_\psi = 0.8 \mid K_i = 0.00066$

These gains were tuned empirically to ensure responsiveness and avoid oscillatory behavior.

The controller was tested under various maneuvers (e.g., constant radius turns, double lane change) and shown to maintain path-following accuracy even during tire deflation events.

5.3 Simulation Maneuvers and Test Conditions

1. Constant Radius Turn

A constant radius highway left turn was simulated at a speed of 22.36 m/s (≈ 80 km/h). The turn radius was computed dynamically using the standard curvature design formula:

$$R = \frac{V^2}{g.f}$$

With $f = 0.15$ and

$$g = 9.81\ \mathrm{m/s^2}$$

The realistic turning radius of 250 meters was used as the basis for the reference trajectory. A total track arc of 650 meters was covered.

Tire deflation was introduced at 13 seconds, switching the front tire model from its inflated Pacejka parameters to the deflated ones. A closed-loop steering controller was used with lateral error and heading correction terms. The same control structure and gains were applied for both standard and run-flat tire simulations.

6. Results of standard tire and runflat tires in terms of vehicle handling.

This section presents and analyses the simulation results obtained from testing both standard and run-flat tire models during a constant-radius turning maneuver, with front-left tire deflation occurring at t=13 seconds. The objective is to compare the dynamic behavior of the vehicle under each tire configuration, particularly focusing on the vehicle's ability to maintain trajectory, generate sufficient lateral forces, manage slip dynamics, and effectively respond through the steering controller. Plots of vehicle path, lateral forces, slip angles, and control input are discussed in sequence for both cases.

6.1 Standard tire: Deflation response to constant radius turn.

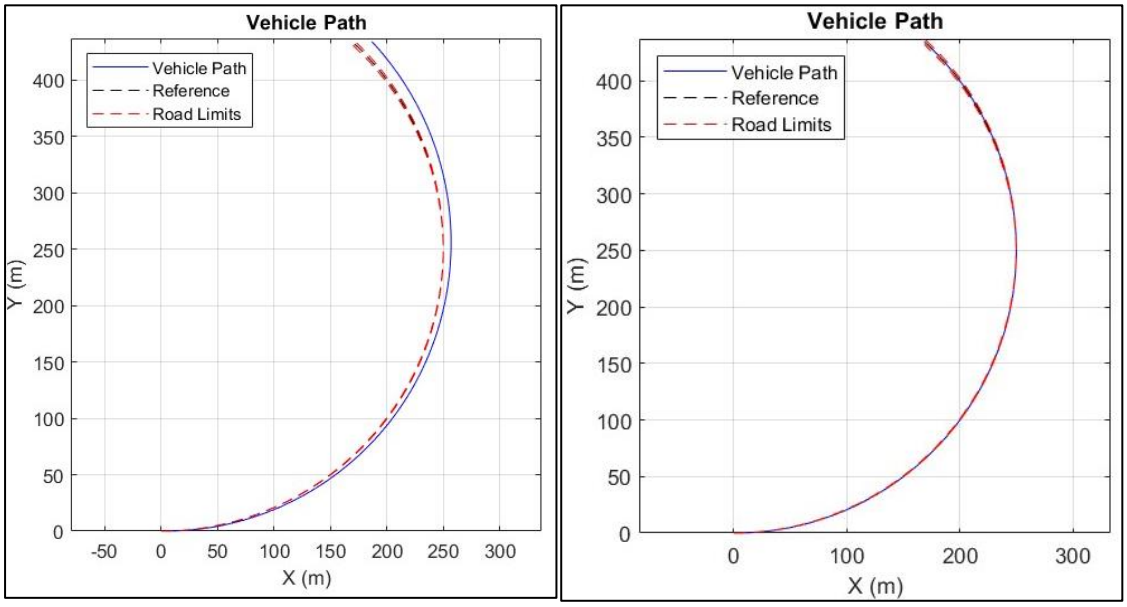

Figure 23: Constant radius turns, left with controller disabled and right with controller enabled.

The response of the vehicle using standard tires under a constant radius turn is shown in Figure 23. In the absence of steering control (left plot), the vehicle deviates from the reference path following deflation. Even with the controller enabled (right plot), the path initially remains within acceptable bounds, but by approximately t=23 seconds, the vehicle

begins to exhibit a sharp increase in lateral error. This deviation escalates rapidly, with the trajectory ultimately diverging more than 10 meters from the desired path, far exceeding the lane boundaries.

This loss of control is closely linked to the tire force dynamics shown in Figure 24. Before deflation, the front-left (FL) and front-right (FR) tires share the lateral load reasonably well, with a higher load on the FR due to expected weight transfer in the right-hand turn. However, after deflation, the lateral force from the FL tire drops sharply, indicating the tire's inability to sustain cornering stiffness. Consequently, the FR tire compensates by increasing its lateral force, but this shift causes it to reach saturation, unable to provide additional steering authority. The rear tires (RL and RR) remain relatively symmetric initially but begin to show imbalance as the front axle destabilizes, further compromising yaw control.

The evolution of tire slip angles further explains the deterioration in handling, as shown in Figure 25. The FL slip angle declines after deflation, reflecting the loss in cornering capability. The FR slip angle, by contrast, increases as the tire tries to compensate, resulting in an asymmetric slip pattern across the front axle. Rear slip angles remain within a manageable range but begin to deviate as the overall system stability degrades.

Figure 26 presents the lateral deviation and steering input over time. A critical observation is the steep growth in lateral deviation after deflation, which peaks beyond the track boundary. Meanwhile, the steering input curve reveals that the controller continuously increases the command angle until it saturates at the pre-defined limit of ±0.4 radians. Despite this maximum input, the steering system is unable to recover stability, demonstrating the limitations of the standard tire under pressure-loss conditions. The yaw rate concurrently

drops below nominal values, indicating reduced turning responsiveness and reduced effective curvature compliance.

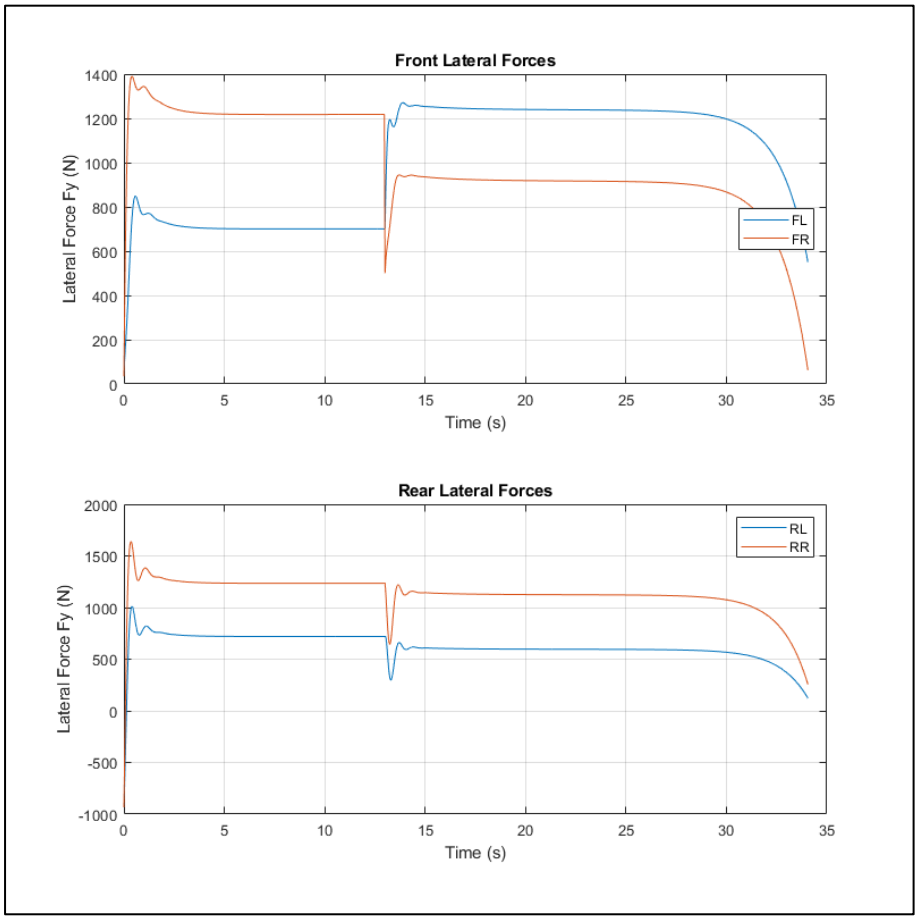

Figure 24 - Lateral Tire forces at the front and rear axle for standard tire.

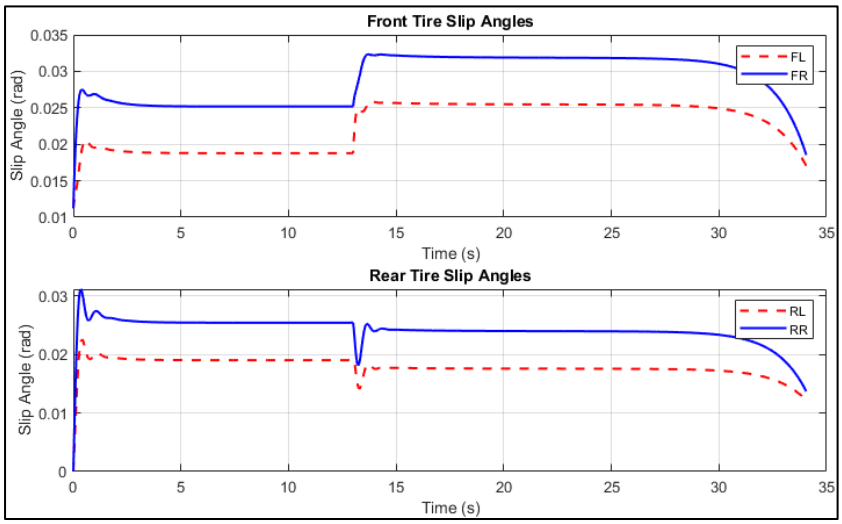

Figure 25 - Slip angles at the front and rear tires for standard tire

.

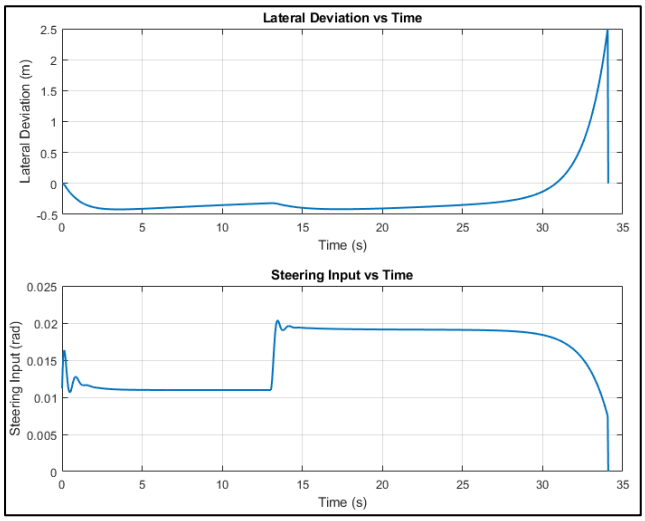

Figure 26 - Overall vehicle lateral deviation (m) and steering input (rad).

6.2 Runflat Tire: Deflation Response to constant radius turn.

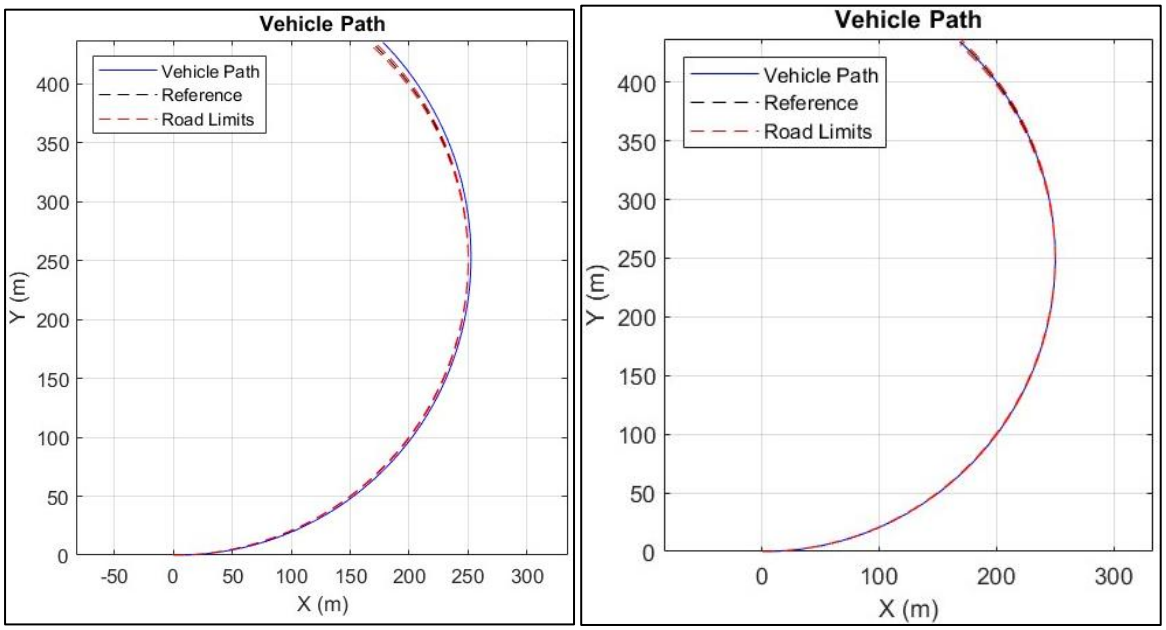

Figure 27: Comparison of vehicle trajectories on a constant-radius path for deflated front-left tire cases—Standard tire (left) and Run-flat tire (right).

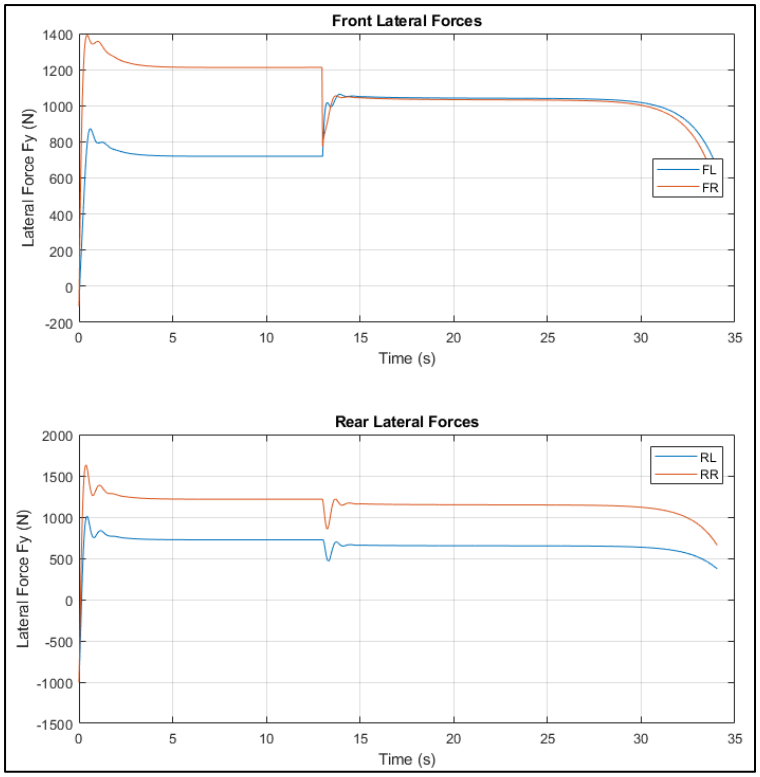

Figure 28 - Lateral Tire forces and vehicle lateral deviation

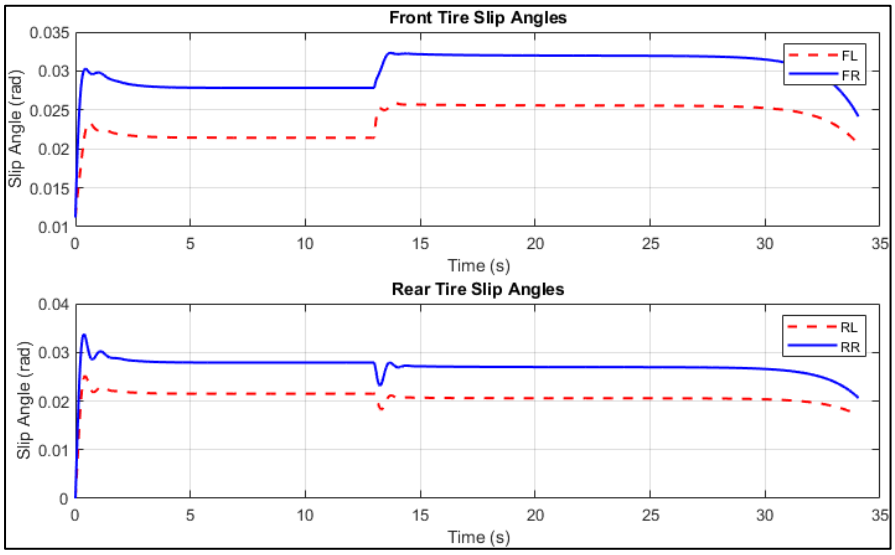

Figure 29 - Slip angles at the front and rear tires for runflat tire.

In contrast, the run-flat tire demonstrates superior performance when subjected to the same deflation scenario. Figure 27 shows that the vehicle remains closely aligned with the reference path throughout the simulation. The trajectory remains bounded within ±0.5 meters of the reference curve, indicating robust lateral tracking performance even after deflation.

There is no sign of divergence or abrupt deviation, and the reference curve is followed with remarkable consistency.

The reason for this enhanced performance becomes clear when examining the tire force distribution in Figure 27. After deflation, the front-left (FL) tire continues to generate a meaningful amount of lateral force. Although its contribution is lower than the pre-deflation level, the presence of a self-supporting sidewall allows the run-flat tire to retain a degree of stiffness and sustain the required force. This prevents the front-right (FR) tire from saturating, as the lateral load is more evenly shared between the front wheels. The rear tires also remain well-balanced and exhibit no major disruptions in force generation.

Slip angle behavior in Figure 29 supports this interpretation. Unlike the standard tire case, the slip angles at the front do not exhibit an abrupt divergence. Both FL and FR tires maintain slip angles within reasonable ranges, which helps ensure smooth yaw dynamics. Similarly, the rear tires continue operating in a stable regime, with symmetric slip angles that reflect a well-balanced response to lateral load transfer.

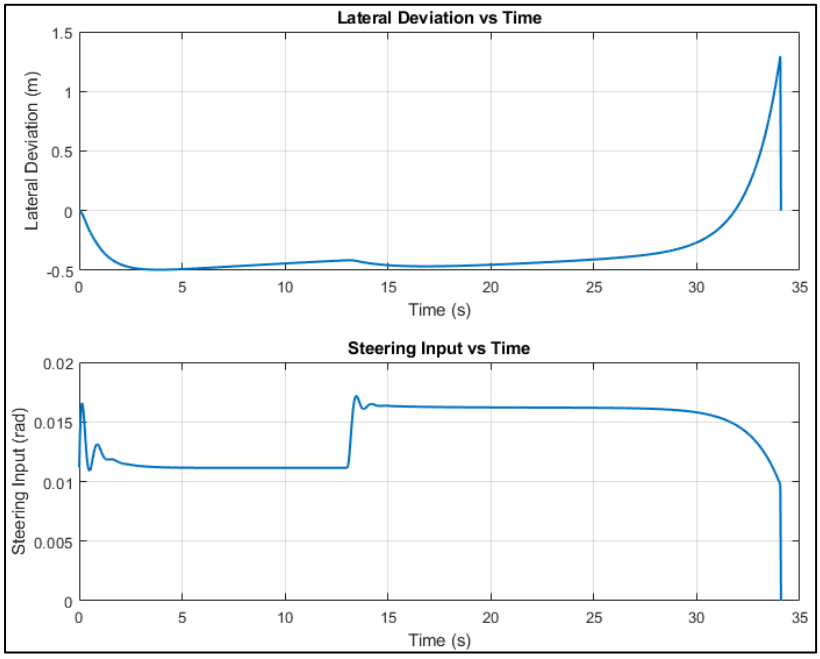

Figure 30 - Overall vehicle lateral deviation (m) and steering input (rad).

Finally, the steering controller’s performance is summarized in Figure 30. The lateral deviation stays stable across the entire simulation period, with no spikes or delayed divergence observed. Moreover, the steering input remains comfortably below saturation levels, suggesting that the controller retained sufficient authority to adjust heading and correct for small deviations. This control margin is indicative of the run-flat tire's ability to support the steering system by preserving cornering force even after deflation.

Overall, the run-flat tire model proves its ability to retain lateral stiffness and maintain stability under deflation. Unlike the standard tire, it does not collapse under the loss of inflation, enabling the vehicle to track the reference path safely and effectively. The integration of stiff sidewalls in the run-flat design plays a key role in preserving force generation and avoiding controller saturation.

7. Conclusion

This thesis investigated the influence of tire structural design specifically, standard pneumatic tires versus self-supporting run-flat tires, on vehicle handling performance under deflation scenarios. A comprehensive simulation-based framework was established, combining finite element tire modelling using Abaqus, empirical force extraction, and vehicle-level analysis through a nonlinear 3-DOF four-wheel vehicle model. The model accounted for individual tire forces using Pacejka-based lateral force equations, load transfer effects, and asymmetries arising from inflation status. Tire force models were developed for four distinct conditions: standard-inflated, standard-deflated, run-flat-inflated, and run-flat-deflated.

Using this framework, high-speed maneuvers, including constant radius turns and double lane change scenarios, were simulated with controlled tire deflation events. Key vehicle dynamics variables such as lateral deviation, yaw rate, slip angles, lateral forces, and steering input were monitored under both open-loop and closed-loop conditions. The closed-loop system incorporated a velocity-scaled proportional-integral steering controller with feedforward curvature compensation and anti-windup logic, designed to emulate autonomous corrective behavior during emergency events.

The results demonstrated that while both tire types maintained stable behavior under inflated conditions, the standard tire exhibited a significant loss of lateral stability following deflation. This was characterized by a sharp reduction in front axle force capacity, saturation of the steering input, excessive lateral deviation from the reference path, and onset of yaw instability. In contrast, the run-flat tire preserved acceptable path-tracking accuracy and dynamic stability post-deflation. The reinforced sidewall construction of the run-flat design enabled it to sustain lateral force generation despite the loss of internal pressure, preventing overload of the opposing front tire and ensuring continued steering authority.

These findings validate the superior lateral handling and safety performance of run-flat tires in pressure-loss scenarios, particularly during high-speed cornering. The simulation results also confirm the robustness of the enhanced vehicle model, which accounted for load transfer and asymmetric tire force generation, in predicting vehicle behavior under deflation conditions. Moreover, the effectiveness of the closed-loop steering strategy in managing path tracking and stability under tire failure conditions was demonstrated. Overall, the study underscores the importance of integrating detailed tire models, including deflation characteristics, into vehicle dynamics analysis to support design and safety evaluations.

While the current framework establishes a robust comparison of deflated tire behavior, several extensions are proposed to enhance the depth and applicability of the study:

1. Combined Slip Modelling: Current simulations are restricted to lateral slip. Incorporating longitudinal slip dynamics would allow analysis of combined braking/cornering conditions, which are more representative of real-world failure scenarios.
2. Alternative Failure Cases: Simulations can be extended to rear tire deflation, diagonal deflation, and asymmetric pressure loss across axles, to observe broader vehicle responses.
3. Enhanced Vehicle Model: Transitioning to a full 4-wheel or 6-DOF vehicle model with suspension dynamics would provide a more comprehensive view of handling and ride quality.
4. Ride Comfort Metrics: Integration of vertical dynamics and vibration response would allow evaluation of ride comfort trade-offs between tire designs.
5. Path-Tracking Under Obstacle Constraints: Inclusion of emergency maneuvers and obstacle avoidance tasks would allow investigation of tire behavior under evasive actions.

6. Adaptive Control Schemes: More sophisticated steering controllers, including model predictive control (MPC) or gain-scheduled feedback, could further improve path recovery under tire failure.

By extending the methodology in these directions, the vehicle-tire interaction can be more fully characterized, further supporting tire design evaluations and the development of advanced safety systems.

8. Bibliography

1. *A look at the history of the pneumatic tire.* **Gooch, L. R.** Online, 2017, Rubber & Plastics News.

2. *THE DEVELOPMENT OF THE PNEUMATIC TIRE AND ITSIMPORTANCE FOR ROAD TRANSPORTATION.* **Burchardt, Jørgen.** Ottawa : s.n., 2008, Sixth International Conference on the History of Transport, Traffic and Mobility (T2M).

3. **Clark, S. K.** Pneumatic Tire. *The Pneumatic Tire.* s.l. : U.S. Department of Transportation/NHTSA, N/A, pp. 619-661.

4. **Williams, Derrest.** *The History of Tires.* s.l. : TreadWright Tires, 2018.

5. **Jansson, V.** *A Literature Study of Rolling Resistance and Its Affecting Factors,.* Stockholm, Sweden : Bachelor's thesis, Dept. of Mechanical Engineering, KTH Royal Institute of Technology, 2022.

6. *Tire with belt between bias carcass plies,.* **Nichols, G. L. Jennings and P. M.** s.l. : U.S. Patent and Trademark Office, 1973.

7. *6.32 - Flexible Composites: Tire and Belt.* **Mukai, U., & Morii, T.** Tokyo, Japan : s.n., 2000, Comprehensive Composite Materials, pp. 625–644.

8. *Finite Element Analysis of Nonuniformity of Tires with Imperfections.* **Jeong, K. M., Kim, K. W., Beom, H. G., and Park, J. U.,.** 3, 2007, Tire Science and Technology,, Vol. 35, pp. 226-238.

9. *Investigation on Mechanical and Temperature Characteristics of Self-Supporting Run-Flat Tire During Pressure Relief.* **Liguo Zang, Tian Lv, Cheng Xue, Fengqi Wei, Weiqiang**

Zhao, Fei Teng. s.l. : Springer, on behalf of The Korean Society of Automotive Engineers, 2024, International Journal of Automotive Technology.

10. *The Self-Supporting Tire: A New Concept In Vehicle Mobility.* **Alden, John T.** Detroit : Society of Automotive Engineers (SAE), 1977.

11. **Veld, I. B. A. op het.** *Run flat tires versus conventional tires: an experimental comparison.* Eindhoven, Netherlands : Technische Universiteit Eindhoven, DCT rapporten Vol. 2006.042, 2006.

12. *Study on the Effect of Different Design Parameters of Sidewall Insert Rubber on the Mechanical Characteristics of Self-Supporting Run-Flat Tires.* **Lv, T., et al.** s.l. : Lubricants, 11(458), 1–17, 2023.

13. *Optimum design of run-flat tire insert rubber by genetic algorithm.* **Cho, J.R., et al.** s.l. : Elsevier, 2011, Finite Elements in Analysis and Design, Vol. 52, pp. 60-70.

14. *Experimental Analysis of a Run-flat Tires for Automobiles.* **C.VenkateshwarReddy, et al.** 2, s.l. : International Journal of Innovative Research in Technology (IJIRT), vol. 9, no. 2, 2022, Vol. 9.

15. *Tests documenting vehicle handling with a temporary use rear tire and a runflat rear tire.* **Arndt, Mark W. and Arndt, Stephen M.** s.l. : SAE International, 2006.

16. *Drag and Steering Effects From.* **Robinette, Ric D. and Fay, Richard J.** s.l. : SAE International, 2000.

17. *Runflat-Technology and its Impact on Design and Durability of Wheels.* **Heim, Ruediger, Krause, Ivo and Weingaertner, Steffen.** Michigan : SAE International, 2007.

18. **Systèmes, Dassault.** Steady-State Transport Analysis. [Online] https://abaqus-docs.mit.edu/2017/English/SIMACAEXARefMap/simaexa-c-rollingtire.htm#simaexa-c-rollingtire-t-bibliography-c1.

19. —. Steady-state rolling analysis of a tire. [Online] 2017. https://docs.software.vt.edu/abaqusv2024/English/?show=SIMACAEANLRefMap/simaanl-c-steadystatetransport.htm.

20. **Pacejka, Hans B.** *Tyre and Vehicle Dynamcis.* s.l. : Elsevier, 2006.

21. *Tire Model Application and Parameter Identification-A Literature Review.* **Bin Li, Xiaobo Yang, James Yang.** 1, s.l. : SAE International, 1 April 2014, SAE International Journal of Passenger Cars – Mechanical Systems, Vol. 7.

22. *A Nonlinear Bike Model for Purposes of.* **Turnwald, A. and Liu, S.** s.l. : Details not fully available in excerpt, 2018, International Federation of Automatic Control.

23. *Using Objective Vehicle-Handling Metrics for Tire Performance Evaluation and Selection.* **Sivaramakrishnan, S. and Taheri, S.** s.l. : Details not fully available in excerpt, 2013, SAE Int. J. Passeng. Cars - Mech. Syst. 6(2).

24. *A tool for tire handling performance evaluation.* **Siramdasu, Y. and Taheri, S.** s.l. : Details not fully available in excerpt, 2016, Tire Science and Technology, Vol. 44, pp. 74-101.

25. **Nazar, Reza N.** *Vehicle Dynamics: Theory and Application.* s.l. : Springer Nature, 2017.

26. *A New Tire Model with an Application in Vehicle Dynamics Studies.* **Bakker, Egbert, Pacejka, Hans B. and Lidner, Lars.** s.l. : SAE International, 1989, Vol. SAE Paper No. 890087, pp. 101-113.

27. *An Analysis of Tire Traction Properties and Their Influence on Vehicle Dynamic Performance.* **Howard Dugoff, P. S. Fancher , Leonard Segel.** s.l. : SAE International, 1970, Vol. 79, pp. 1219-1243.

28. *Analysis of mechanical characteristics of inserts supporting run-flat tire during pressure relief.* **Xingyu Wang, Liguo Zang, Zhi Wang, Zhendong Zhao, Fen Lin, Fei Teng.** s.l. : Springer, April 2021, Journal of the Brazilian Society of Mechanical Sciences and Engineering, Vol. 43.

29. *Analytical Tire Models for Dynamic Vehicle Simulation.* **CAPTAIN, K. M., BOGHANI, A. B. and and WORMLEY, D. N.** 1, London : Taylor & Francis, July 1979, Vehicle System Dynamics: International Journal of Vehicle Mechanics and Mobility [online]., Vol. 8, pp. 1-32.

30. **Gillespie, Thomas D.** *Fundamentals of Vehicle Dynamics.* s.l. : Society of Automotive Engineers, 1992.

31. *Innovative Run Flat Systems.* **Piotr Stryjek, Tomasz Nikisz, Krzysztof Omyliński, Jerzy Ejsmont.** 1, s.l. : Journal of KONES Powertrain and Transport, 2015, Vol. 22.

32. *Optimize Design of Run-Flat Tires by Simulation and Experimental Research.* **Huaqiao Liu, Yiren Pan, Huiguang Bian, Chuansheng Wang.** 3, s.l. : MDPI, 20 January 2021, Materials, Vol. 14.

33. **Milliken, William F. Milliken and Douglas L.** *Race Car Vehicle Dynamics.* s.l. : SAE International, 1995.

34. *Research on Operational Characteristics of Tyres with Run Flat Insert.* **Grzegorz Motrycz, Piotr Stryjek, Jerzy Jackowski, Marcin Wieczorek, Jerzy Ejsmont, Grzegorz**

Ronowski, Sylwia Sobieszczyk. 3, s.l. : Journal of KONES Powertrain and Transport, 2012, Journal of KONES Powertrain and Transport, Vol. 19.

35. *Ride Comfort Evaluation of Bias Ply and Radial Run - Flat Tire in High Mobility Vehicle.* **W. S. Khan, F. A. Dar.** Pune, India : SAE International and SAE India, N/A. Symposium on International Automotive Technology (SIAT) 2013.

36. **Pacejka, Hans B.** *Tyre and Vehicle Dynamics.* 2. United Kingdom : Butterworth-Heinemann, 2006.

37. *Tyre Modelling for Use in Vehicle Dynamic Studies.* **Egbert Bakker, Lars Nyborg, Hans B. Pacejka.** Section 2, s.l. : SAE International, 1987, SAE Transactions, Vol. 96, pp. 190-204.

38. **Jazar, Reza N.** *Vehicle Dynamics Theory and Application.* 3. s.l. : Springer International Publishing AG, 2017.

39. *Vehicle dynamics and tire models: An overview.* **Mohamed Belrzaeg, Abdussalam Ali Ahmed, Amhimmid Q Almabrouk, Mohamed Mohamed Khaleel, Alforjani Ali Ahmed, Meshaal Almukhtar.** 1, October 2021, World Journal of Advanced Research and Reviews, Vol. 12, pp. 331-348.

40. *Vehicle Stability Control System for Enhancing Steerability, Lateral Stability, and Roll Stability.* **J.-S. Jo, S.-H. You, J. Y. Joeng, K. I. Lee, K. Yi.** 5, s.l. : Korean Society of Automotive Engineers (KSAE), 2008, Internation Jounel of Automotive Technology, Vol. 9, pp. 571-576.

41. *Review on self-inflation tire system.* **Debajeet Mohapatra, Shikha Parashar.** s.l. : Elsevier, 2023, Materials Today: Proceedings, Vol. 81, pp. 346–349.

42. *Properties of Tires Affecting Riding, Steering and Handling.* **Evans, R. D.** s.l. : SAE International, 1935, SAE Transactions, Vol. 30, pp. 41-49.

43. *Analysis of Load Characteristic and Contact Patch Characteristic of Support Insert Run-Flat Tire Under Zero-Pressure Condition.* **Zang, Liguo, et al.** s.l. : Korean Society of Automotive Engineers, 2021, International Journal of Automotive Technology, Vol. 22, pp. 1141-1151.

9. Appendix

9.1 MATLAB Code for fitting Pacejka Coefficients

```
clear;
clc;

filename = 'TireData.xlsx';
sheets = {'runflat_inflated', 'standard_inflated', 'runflat_deflated',
'standard_deflated'};

% Pacejka lateral force function
pacejkaFy = @(x, alpha) x(3) .* sin(x(2) .* atan(x(1) .* alpha - x(4) .*
(x(1) .* alpha - atan(x(1) .* alpha))));

% Initial guess and bounds [B, C, D_normalized, E]
x0 = [15, 1.5, 1, 0.9];
lb = [0 0.8 0 0];
ub = [100 2.5 5 1];

% Optimization options
options = optimoptions('lsqcurvefit', 'Display', 'off', ...
    'MaxFunctionEvaluations', 5000, 'MaxIterations', 2000);

% Structure to store results
pacejka_coeffs2 = struct();

%% === Loop Over All Sheets ===
for i = 1:length(sheets)
    sheet = sheets{i};
    data = readtable(filename, 'Sheet', sheet);

    % Extract slip angle and lateral force
    if any(strcmpi(data.Properties.VariableNames, 'Fy'))
        Fy = data.Fy;
    else
        error('Column "Fy" not found in sheet: %s', sheet);
    end

    alpha_deg = data.SlipAngle;
    alpha_rad = deg2rad(alpha_deg);

    % === Flip the sign of Fy to match expected tire physics ===
    Fy = -Fy;

    % === Keep only valid rows (nonzero & finite) ===
```

```
    valid_idx = isfinite(alpha_rad) & isfinite(Fy) & ~(Fy == 0 & alpha_deg
~= 0);
    alpha_rad = alpha_rad(valid_idx);
    Fy = Fy(valid_idx);

    if isempty(Fy)
        warning('%s: No valid data found for fitting.', sheet);
        continue;
    end

    % === Normalize Fy ===
    Fy_max = max(abs(Fy));
    Fy_norm = Fy / Fy_max;

    % === Fit Pacejka to normalized data ===
    [x_fit_norm, ~] = lsqcurvefit(@(x, alpha) pacejkaFy(x, alpha), ...
        x0, alpha_rad, Fy_norm, lb, ub, options);

    % === Rescale D ===
    x_fit = x_fit_norm;
    x_fit(3) = x_fit(3) * Fy_max;

    % Store results
    coeffStruct = struct('B', x_fit(1), 'C', x_fit(2), 'D', x_fit(3), 'E',
x_fit(4));
    pacejka_coeffs2.(sheet) = coeffStruct;

    % Plot
    alpha_fit = linspace(min(rad2deg(alpha_rad)), max(rad2deg(alpha_rad)),
200);
    Fy_fit = pacejkaFy(x_fit, deg2rad(alpha_fit));

    figure;
    plot(rad2deg(alpha_rad), Fy, 'bo'); hold on;
    plot(alpha_fit, Fy_fit, 'r-', 'LineWidth', 2);
    title(['Lateral Force Fit - ', strrep(sheet, '_', '\_')]);
    xlabel('Slip Angle (deg)');
    ylabel('Lateral Force Fy (N)');
    grid on;
end
```